DNA Methylation Underlies the Long-Term Association Between Oral *Porphyromonas gingivalis* infection and Atherosclerotic Cardiovascular Disease

by

Mohamed Omar

A thesis submitted in partial fulfilment of the requirements for the degree of

Doctor of Philosophy

Medical Sciences – Periodontology

University of Alberta

Abstract

Objective: Periodontitis, one of the most common inflammatory conditions, and the leading cause of teeth loss in adults, has been associated with cardiovascular disease (CVD) for decades, and has recently been identified, by the American Heart Association, as an independent risk factor for atherosclerotic CVD. Importantly, periodontitis is a chronic condition without a definitive treatment endpoint, and patients are managed by regular scaling and root planning. This inherent limitation renders the assessment of the effect of periodontitis treatment on the increased risk of CVD quite challenging. However, long-term studies in edentulous patients with history of periodontitis, showed persistence of the increased CVD risk for years after edentulism, suggesting that clinical elimination of the disease might not be sufficient in decreasing the periodontitis-induced CVD risk. In this project we sought to explore the validity and nature of this suggested long-term association.

Hypothesis: We hypothesized that periodontitis induces some epigenetic changes, in the form of DNA-methylation, in hematopoietic stem cells in the bone marrow, and such changes persist after clinical elimination of the disease, and underlie the induced-CVD risk.

Methods and Results: Using the atherosclerotic mouse model, the low-density lipoprotein receptor Knock out ($LDLR^{-/-}$), all mice were fed a high fat diet (HFD) to induce atherosclerosis. Oral inoculation with *Porphyromonas gingivalis* (*pg*), a key stone periodontal pathogen, was used to induce periodontitis in one group of mice, whereas the other group was sham inoculated. Our lab has previously shown that mice that were fed a HFD and inoculated with *Pg* developed more atherosclerosis than mice that were sham-inoculated. To simulate clinical elimination of periodontitis and persistence of the hypothesized epigenetic

reprogramming, we used a bone marrow transplant approach. Naïve *LDLR*$^{-/-}$ mice were irradiated and transplanted with bone marrow cells form HFD fed mice that were either *Pg*-inoculated or sham-inoculated, creating two groups of recipient mice. Aorta morphometry showed that, like the donor mice, mice recipient of bone marrow from *Pg*-inoculated donors developed significantly more atherosclerosis compared to mice recipient of bone marrow from sham-inoculated donors. This increase in atherosclerosis was accompanied with a more pro-inflammatory plasma and macrophage cytokine profile. We hypothesize that changes in DNA methylation, could in part, underlie the observed increase in atherosclerosis. This was tested using whole genome bisulphite sequencing (WGBS) approach, the gold standard for a thorough and quantitative assessment for DNA methylation of the entire genome. Our data show a significant difference in the methylation profile of peritoneal macrophages between the two groups of recipient mice. There was 375 identified differentially methylated regions (DMRs) between the groups, with global hypomethylation in mice recipients of bone marrow from *Pg*-inoculated donors. Some of the DMRs pointed to the involvement of enzymes with major roles in the methylation and demethylation process. In mice recipients of bone marrow from *Pg*-inoculated donors, methionine adenosyl transferase (MAT), which catalyzes the conversion of methionine to *S*-adenosylmethionine (SAM), the universal methyl-donor, was hypermethylated. The protein coding gene for S-adenosylhomocysteine hydrolase (SAHH), which catalyzes the reversible conversion of the potent methylation inhibitor, S-adenosylhomocysteine (SAH), to homocysteine and adenosine was also hypermethylated. In contrast, the de-methylation enzyme, Ten-Eleven Translocase (TET 2), was hypomethylated. Accordingly, we sought to investigate the mechanism underlying the observed global hypomethylation and its potential association with the observed increase in atherosclerosis. In line with the global hypomethylation, our

activity assays showed a significant increase in TET activity and a decrease in DNA methyltransferases (DNMT). In addition, plasma SAH levels were significantly higher and SAM to SAH ratio was decreased, both of which have been associated with CVD and with increased risk of myocardial infarction and stroke.

Significance: Homocysteine, is located at the intersection of the methionine cycle and the trans-sulphuration pathway, where it can either be re-methylated to methionine and go through the methionine cycle, or it can synthesize cysteine through the trans-sulphuration pathway. Glutathione (GSH), a critical antioxidant, is the end-product of the trans-sulphuration pathway. Hence, as a coping mechanism, the trans-sulphuration pathway is favoured over the methionine cycle under conditions of oxidative stress. Importantly, periodontitis has been repeatedly shown to induce oxidative stress.

In this dissertation, we are submitting a novel and a paradigm shifting mechanism in the long-term association between periodontitis and atherosclerotic CVD. We propose that periodontitis-induced oxidative stress leads to global DNA hypomethylation through disruption of the methionine cycle, and that the resultant increase in SAH increases the risk of atherosclerotic CVD.

Preface

Study design, and planning and development of experiments were done in collaboration with Dr. Febbraio. I was responsible for morphometric analysis, RNA collection, cDNA synthesis, qPCR, cytokine array, DNA purification for sequencing, cell culture and activity assays. Dr. Febbraio and Dr. Alexiou helped in irradiation, bone marrow transplants, and blood and tissue collection. Konrad Lehman, a previous student in Dr. Febbraio's lab, helped in making the cell culture media (L929 Conditioned Media)and developing the protocol to generate bone marrow derived macrophages. The flow cytometry experiment to test our irradiation and transplant efficacy was done by Cole Delyea, a student in Dr. Shokrollah Elahi's lab. All animal procedures were approved by the University of Alberta Animal Care and Use Committee under animal use protocol # 570 (Febbraio; approved in 2013 and renewed in 2017).

Dedication

I would like to dedicate this dissertation and all the effort and time invested in completing it to my parents, Dr. Eman Alsukkary and Mr. Ahmad Omar, whom their unmatched support was a cornerstone for all my studies and successes. This is as well dedicated to my wonderful wife, Sara, and to my gorgeous daughter, Laila, they made the journey much more exciting and enjoyable. Last but not least, I am dedicating this dissertation to my siblings, Rana, Omar and Arwa.

Acknowledgements

I would like to sincerely express my appreciation and gratitude to my mentor and supervisor, Dr. Maria Febbraio, for her unconditional support and for her quintessential supervision throughout my studies. Your sincere efforts and keenness to provide the best opportunity to your students have had tremendous impact on my professional as well as on my personal life, an impact I would cherish for life. I would like to recognize my committee members, Dr. Patrick Flood and Dr. Daniel Graff, for their guidance and their constructive criticism and feedback throughout the years. I would like to thank my arms-length and external examiner, Dr. Jhon Usher and Dr. Edward Putnins for their time and insight. Special thanks to Dr. Maria Alexiou for her help with experiments and for teaching me some of the basic and fundamental concepts in research.A big thank you to my all fellow lab members: Dr. Raisa Catunda, Konrad Lehmann, Dr. Umar Rekhi, Danielle Clark, Aneesh Bhardwaj, Zahra Mantaka, Dr. Yuli Berlin-Broner, Julia Piche, and Karen Ho for all their support throughout the journey.

I would like as well to thank my co-residents Dr. Salar Mofidi, Dr. Dongdong Fang and Dr. Hessam Tehrani for their continuous support during my Periodontology clinical training and thereafter. A very special thank you to Dr. Jim MacDonald for his dedication and exceptional clinical training he offered during my clinical residency. Just over a decade ago, I had my first class in Periodontology with Dr. Noha Ghallab, and her phenomenal teaching strategies initiated my passion for Periodontology and inspired me to specialize in the field, and for that I am grateful. A final thank you to the funding sources that made this study possible: The Faculty of Medicine and Dentistry, and the School of Dentistry (Fund for Dentistry Grant), CIHR, and The Heart and Stroke Foundation.

Table of Content

List of Figures

List of Abbreviations

AA- Aggregatibacter actinomycetemcomitans

AAP - American Academy of Periodontology

Apo - apolipoprotein

bp - basepair

BMDM – bone marrow-derived macrophages

CBS - cystathionine β-synthetase

CRP - C-reactive protein

CpG - cytosine-guanine

CVD – cardiovascular disease

DNMT - DNA methyltransferases

DMP – differentially methylated promoter

DMR – differentially methylated region

DMSO – dimethyl sulfoxide

DMEM - Dulbecco's Modified Eagle Media

EDTA - ethylenediaminetetraacetic acid

FBS – fetal bovine serum

FDR – false discovery rate

G-CSF - Granulocyte – Colony Stimulating Factor

GSH - Glutathione

Gy – Gray

HFD – high fat diet

HIV- human immunodeficiency virus

IL – interleukin

ICAM - intercellular adhesion molecule

IP – intra-peritoneal

IMDM - Iscove's Modified Dulbecco's Media

kb - kilobase

LCCM - L929 Conditioned Cell Media

LDL – low-density lipoprotein

LDLR – low density lipoprotein receptor

LPS - lipopolysaccharide

NHANES 1 - First National Health and Nutrition Examination Survey

Ox-LDL - Oxidized-LDL

p_{adj} – adjusted p-value

PBS – phosphate buffered saline

PCR – polymerase chain reaction

Pg - Porphyromonas gingivalis

ROS – reactive oxygen species

RPMI - Roswell Park Memorial Institute

SAM - *S*-adenosylmethionine

SAH - S-Adenosylhomocysteine

SAHH - S-Adenosylhomocysteine hydrolase

TET - Ten-Eleven Translocase

TIMP - Tissue Inhibitor of Metalloprotenase

TNF - tumor necrosis factor

TLR - Toll-like receptor

TREM - Triggering Receptors Expressed on Myeloid Cells

VCAM - vascular cell adhesion molecule

VLDL – very low-density lipoprotein

WGBS – whole genome bisulphite sequencing

WT – wildtype

5hmC - 5-hydroxymethylcytosine

5mC- methylated cytosine

List of Symbols

♂ - male

♀ - female

$^{-/-}$ - knockout

CHAPTER 1

Introduction

Periodontal Disease

The periodontium is the support apparatus of teeth; it is composed of cementum, periodontal ligament, bone and gingiva[1]. This apparatus functions to attach cementum, the outer layer of teeth, to alveolar bone, through the periodontal ligaments. Another critical function is that it acts as barrier to protect the underlying structures, namely cementum, periodontal ligaments and alveolar bone, from the oral microflora[1]. This barrier function is primarily fulfilled through the connective tissue attachment between the gingiva and the tooth. In fact, the integrity of this connective tissue attachment is the differentiating factor between a healthy and diseased periodontium[1].

Periodontitis, as the name suggests, is a disease characterized by inflammation of the periodontium. The disease starts by loss of the connective tissue attachment and manifests with signs of gingival inflammation including bleeding, erythema and possibly gingival enlargement, which is followed by gradual loss of alveolar bone, followed by tooth mobility and eventually tooth loss[2,3]. The primary etiology of this disease is oral bacteria in a susceptible host[3,4]. The first part of the etiology, the oral bacteria, is the main constituent of the periodontal biofilm which is constantly covering teeth surfaces. Despite the fact that the periodontal biofilm constitutes more than 700 diverse bacterial species[5], there are specific bacteria that have been associated with periodontal destruction, including bacteria of the Red Complex, *Porphyromonas gingivalis* (*Pg*)*,* *Treponema denticola,* and *Tannerella forsythia,* some bacteria of the Orange Complex, such as *Prevotella intermedia* and other bacteria like *Aggregatibacter actinomycetemcomitans (AA),* all of which are anaerobic and gram negative[6-8]. These observations and associations drove the evolution of the specific plaque hypothesis, which states that the constituent of the periodontal plaque rather than the amount is the driving factor for disease initiation[9]. In other words, it's the

quality of plaque rather than quantity. These so-called periodontal pathogens possess virulence factors that enable them to evade and overcome the host immune response and invade into deeper tissues. The fact that these species are anaerobic gives them the advantage of surviving in the subgingival low-oxygen environment. *Pg* is thought to be a keystone periodontal pathogen because of its ability to shift a benign microbiota into a dysbiotic one, without necessarily being the most abundant in number[9]. Through gingipains and flagella, *Pg* attaches firmly to soft and hard tissue and invades through deeper subgingival structures[8,11,12]. Another critical virulence factor possessed by *Pg*, is lipopolysaccharide (LPS), which induces macrophages to release nitrous oxide and secrete pro-inflammatory cytokines such as interleukin (IL)1-β and tumor necrosis factor (TNF)-α[8,11,12].

The second part of the etiology, the host, or more specifically, the susceptibility of the host, determines the occurrence of the disease as well as the severity and rate of progression, and in some cases even the response to treatment. In a classical study on Sri Lankan tea-workers, researchers found that despite similar levels of poor oral hygiene and similar quality and quantity of periodontal plaque, 11% of the population didn't develop periodontitis or had very slow progression, whereas 8% of the population developed severe periodontitis and showed up to ten times more rapid progression of the disease[13-15]. The susceptibility is determined by several factors, including genetics, such as an IL-1 polymorphism which renders individuals more susceptible to periodontitis[16,17], a medical condition, where uncontrolled diabetics are more susceptible than controlled diabetics or healthy individuals[18-20], as well as smoking[21-23]. In fact, diabetes mellitus and smoking have been shown through longitudinal studies to be independent risk factors for periodontitis[1].

This evolving information about difference in disease severity, susceptibility and rate of progression, as well as the risk factors, have always challenged the different diagnostic systems and classifications proposed by the American academy of Periodontology throughout the previous decades[24,25]. The most recent world workshop by the American Academy of Periodontology (AAP) and the European Federation of Periodontology introduced a dynamic multi-dimensional staging and grading system that incorporates disease severity, rate of progression and risk factors, which allows for personalized approach to patient care[27-37].

The treatment of periodontal disease is logically targeted against the etiology, mainly the periodontal bacteria, as well as controlling some of the modifiable risk factors, such as diabetes and smoking. The goal of periodontal treatment is to stop active disease by eliminating or reducing periodontal pathogens through periodic professional dental cleaning, referred to as scaling and root planning, as well as proper oral hygiene[38-42]. However, for the majority of cases the destruction is irreversible, with few exceptions, where regenerative procedures are indicated and successful. Furthermore, even after treatment of periodontal disease, patients should be monitored and evaluated regularly and never treated as patients who had never had periodontitis[43-46]. The reason being is that these patients sustain a higher risk of re-developing periodontitis and further destruction whether due to non-clinical long-term effects of the disease or due to their original predisposition and susceptibility, or both. In this context the America Academy of Periodontology states "*A periodontitis patient is a periodontitis patient for life"*[26].

In a 1976 classical study, Page & Schroeder divided periodontal disease into four stages based on clinical and histological features as well as immune response[47]. The four stages are initial, early, established and advanced, where the initial stage is evident only histologically

without any clinical symptoms, the early and established lesions represent mild to severe reversible gingivitis, then the established lesion is irreversible periodontitis[47].

In the initial lesion, which occurs after 2-4 days of plaque accumulation, there is not any clinical signs of inflammation. Histologically, there is predominance of leukocytes, mainly neutrophils, and an increase in gingival crevicular fluid (GCF). The increase in neutrophil results from the production of the chemoattractant, IL-8, by gingival fibroblasts and epithelial cells. Lipoteichoic acid and peptidoglycans present in the cell wall of early bacterial colonizers, activate complement via the alternative pathway, resulting in production of C3a and C5a[48]. In turn, they induce the release of vasoactive amines from mast cells, resulting in increased vascular permeability and vascular oedema. Mast cells and neutrophils secrete TNF-α, IL-1 and IL-17[48].

The first clinical signs are evident in the early lesion, which occurs after 4-7 days of plaque accumulation[47]. In this stage there is an increase in lymphocytes and macrophages. In fact, lymphocytes, mostly T-cells, make up ~ 70% of the inflammatory infiltrate[47]. CD 4 cells release interferon-gama (IFN-γ) which signals for recruitment of macrophages and their pro-inflammatory polarization (M1 macrophages)[48]. Further, there is an increase in cell adhesion molecules, such as endothelial cell leukocyte adhesion molecule -1 (ELAM-1) and intercellular adhesion molecule-1 (ICAM-1)[48]. At this stage, the vascular changes are more pronounced and ~ 60-70% of the collagen within the infiltrated zone is degraded. Clinically, the gingiva is slightly erythematous with variable degree of bleeding on probing[47].

The established lesion, which occurs after ~ 21 days of plaque accumulation, is characterized by the predominance of plasma cells[47]. There is overt inflammation and apical migration of junctional epithelium. The principal immunoglobulin (Ig) class produced in the

periodontal tissues is IgG, followed by IgM and some IgA[48]. This stage represents moderate to severe gingivitis. Macrophages can either control inflammation and limit the pathological alterations of soft tissue, or intensify the inflammatory response inducing further destruction. Hence, depending on the host susceptibility, some individuals may progress to the advanced stage, which is periodontitis, in few days, weeks, months or years, whereas others may never develop periodontitis. In cases where the inflammatory process is rather intensified and becoming chronic, there is further destruction of the connective tissue, periodontal ligament and alveolar bone. In the advanced stage, there is continuous proliferation of neutrophils and production of inflammatory cytokines and perpetuation of the inflammatory process resulting in irreversible loss of connective tissue attachment and bone destruction[47,48].

Toll-like- receptors (TLR), a class of pathogen recognition receptors, expressed on the membrane of various immune cells including macrophages, detect several pathogen-associated molecular patterns (PAMP) including LPS, flagellin and bacterial lipoproteins[49]. In oral tissues, there is a predominance of TLR-2 and TLR-4. Upon recognition of periodontal pathogen PAMP, macrophage-associated TLRs, through the NF-κB pathway, release several cytokines, including IL-6, IL-1β and TNF-α[49]. IL-6 and IL-1β are biomarkers of periodontitis and are characteristic of the innate immune response[50]. They play fundamental roles in inflammatory cell migration and are as well involved in osteoclastogenesis[49,50]. In the pathogenesis of periodontitis, TNF-α plays multiple roles ranging from inflammatory cell recruitment to direct tissue destruction. It has been shown to upregulate adhesion molecules ELAM-1 and ICAM-1, as well as IL-1β and IL-6. A positive correlation between TNF-α and matrix metalloproteinases (MMPs) suggests a role in degradation of extracellular matrix[49]. Indeed, destruction of the extracellular matrix is another function of macrophages in periodontitis[49]. MMPs are a family of enzymes involved in

degrading extracellular matrix and the basement membrane, their activity is regulated through balance with their endogenous inhibitors, tissue inhibitors of MMPs (TIMPs)[49]. Importantly, IL-6, IL-1β, and TNF-α are the main stimulatory cytokines for MMPs[49,51]. Altogether, macrophages are key players in the pathogenesis of periodontal disease throughout the different stages of the disease, from the early lesion of reversible gingivitis to the advanced lesions of chronic periodontitis.

Atherosclerotic Cardiovascular Disease

Atherosclerosis is a chronic inflammatory condition that is the leading cause of cardiovascular disease (CVD) wherein underlying sub-endothelial plaques can lead to luminal occlusion and obstruction of vital organs, mainly the heart and brain[52]. From 2016 to 2017, the average cost of CVD in the United States amounted to $363.4 billion[53]. CVD refers to a wide spectrum of vascular illnesses, with myocardial infarctions and strokes accounting for the majority of CVD-related mortality and morbidity[52]. According to the American Heart Association, more than 49% of the American population has been diagnosed with one or more forms of CVD[53]. CVD is the greatest cause of mortality in America, accounting for 30.8 percent of fatalities and taking 2200 lives per day, and accounts for approximately 18 million deaths annually worldwide[52,53]. The vast majority of cardiovascular deaths result from the erosion or rupture of atherosclerotic plaque in the arterial wall which is followed by an occluding thrombus. In Canada, just after malignancy, CVD is the second leading cause of death, accounting for 20% of total deaths in the country[54,55]. Paradoxically, even with the emergence of lipid-lowering medications and ongoing studies into the genesis and pathophysiology of the illness, the CVD death rate climbed by a 21.1 percent in the previous decade[52]. This indicates that the tremendous efforts and expenditure, which amounted to 13.6 billion dollars in Canada in one year[56], were not

sufficient to keep up with the dramatic increase in disease incidence and fatality. These alarming numbers highlight the criticalness of CVD and accentuate the need for further research into the disease pathophysiology, to identify and better understand new and established risk factors. The development of atherosclerosis is complex in the sense that several risk factors interact to enhance the likelihood of the disease occurrence or worsening an existing condition. Age, smoking, a high fat diet, and systemic illnesses such as hyperlipidemia, hypertriglyceridemia and diabetes are well-established risk factors[57-64].

Foam cells and fatty streaks are the building units of the atherosclerotic plaque[65]. The inner wall of all blood vessels, arteries, veins and capillaries, is lined by a single layer of endothelial cells, forming the endothelium responsible for exchanges between the bloodstream and the surrounding tissues, in addition to its role in vasodilation. Throughout the years and as atherosclerotic risk factors increase, the endothelium gets injured and this injury impairs its function[66,67]. The endothelium partially loses its vasodilatory capacity altering the necessary vascular flexibility, which in turns disrupts blood flow through the affected artery[66,67]. This disruption induces the release of pro-inflammatory cytokines and signals for recruitment of neutrophils and macrophages to the inflammatory site[66,67]. Simultaneously, endothelial cells express adhesion molecules such as intercellular adhesion molecule (ICAM)-1 and vascular cell adhesion molecule (VCAM)-1, which engage with the leukocytes and allow for firm adhesion and transendothelial migration[68]. The accumulation of leukocytes and retention of lipoproteins result in the formation of lipid-rich foam cells[65].

Similar to their involvement in periodontal disease, macrophages are key players and have a decisive role in all stages of atherosclerosis, including initiation, progression and even resolution[69]. This is owed to a high degree of plasticity that enables them to tailor their response

according to the various microenvironmental stimuli. This observation led to the classification of macrophages into pro-inflammatory and anti-inflammatory phenotype, based on the activation stimuli and the resultant response. The pro-inflammatory macrophages, known as M1, differentiate in response to signalling by IFN-γ and TLR, and are induced by lipoprotein and LPS[69]. In contrast, the anti-inflammatory macrophages, known as M2, differentiate in response to IL-4 and IL-13[69,70]. M1 macrophages carry out their functions by secreting pro-inflammatory mediators including IL-1β, IL-23, TNF-α, CXCL9, CXCL10 as well as through production of high levels of ROS, whereas M2 macrophages carry out their functions by secreting anti-inflammatory mediators such as IL-10 and IL-1 Receptor Antagonist (Ra)[69]. M1 macrophages have been repeatedly shown to be enriched in progressing atherosclerotic plaque, in contrast to M2 macrophages that are involved in repair and remodelling and hence were enhanced in regressing plaque.[71] Due to the complex microenvironment of atherosclerotic sites, which is composed of modified lipoproteins and inflammatory mediators, in addition to necrotic and apoptotic cells, the macrophage population is widely heterogenous[69]. Macrophage foam cells play an important role in the onset and progression of atherosclerosis. The development of these cells is linked to an imbalance in cholesterol inflow, esterification, and efflux[72]. Very low-density lipoprotein (VLDL), the precursor of low-density lipoprotein (LDL) particles is mostly composed of triglycerides and cholesterol and is generated by the liver. VLDL is one of the body's principal routes for tissue lipid delivery. Cholesterol uptake is a process in which macrophages consume extracellular LDL through receptor-mediated phagocytosis and pinocytosis[73]. This mechanism has been linked to Scavenger Receptors (SR) such SR-A and CD36[73]. CD36 and SR-A account for 75 to 90 percent of LDL uptake by macrophages *in vitro*, whereas other SRs fail to compensate for their absence[74]. The low-density lipoprotein receptor

(LDLR) pathway normally regulates LDL cholesterol absorption and droplet size in tandem[75]. In atherosclerosis, endothelial cells and the M1 macrophages, releases excessive ROS which generates a modified form of LDL known as Oxidized-LDL (ox-LDL)[76,77]. Ox-LDL circumvents regulation through bypass of the LDLR pathway[78]. Uncontrolled absorption of ox-LDL, excessive cholesterol esterification, and/or hindered cholesterol release result in a buildup of cholesterol ester stored as cytoplasmic lipid droplets, which causes foam cell formation[73]. When the input and esterification of cholesterol rise and/or the outflow of cholesterol decreases, macrophages eventually convert into lipid-laden foam cells[73], the archetypal cells in atherosclerotic plaque. Further foam cell development, recruitment of T cells and B cells, and the development of a fibrous cap from extracellular matrix, all contribute to the advancement of the lesion[79,80]. As inflammation progresses, along with apoptosis and necrosis of foam cells and immune cells, the fibrous cap diminishes and weakens and eventually raptures releasing pro-thrombotic factors into the blood stream[81]. In turn, this leads to clot formation responsible for myocardial infarctions, strokes and tissue ischemia.

The Association Between Periodontal Disease and Atherosclerotic Cardiovascular Diseases

For decades, there had been a lot of interest in studying and identifying links between the oral cavity and systemic health. Attempts and achievements have been made in identifying salivary biomarkers and clinical manifestations of systemic conditions. Today, the association between oral health and systemic conditions is conceptually well established, and manifests in various forms. There are many conditions that develop intra and extra orally, such as lichen planus, erythema multiforme, pemphigus vulgaris and others[82]. A different form of clinical association is oral manifestations of systemic diseases. One example is oral manifestations of human immunodeficiency virus (HIV), where some patients may develop intra-oral lesions, such

as oral hairy leukoplakia and candida infections, or suffer from xerostomia[82]. Importantly, over the last two decades, there has been a lot of interest in the scientific community in the probable link between periodontitis and atherosclerotic CVD. Several epidemiological and experimental studies have identified an association between periodontal disease and CVD[83]. In 2012, the American Heart Association concluded that "periodontal disease is associated with atherosclerotic vascular disease independent of known confounders"[84]. In other words, periodontitis is now recognized as an independent risk factor for atherosclerosis. The strength of association between the two conditions varies widely between studies due to the inevitable heterogeneity in study design and in clinical measurements and biomarkers used to identify periodontitis. The multiple asynchronous burst progression of periodontal disease, which suggests that several sites have repeated bursts over a finite period of time then prolonged periods of inactivity[85], renders accurate identification of biomarkers even more challenging. A recent meta-analysis concluded that periodontal disease is associated with a 24–35 percent increase in the risk of coronary heart disease and CVD events[86]. In 2016, a large case-control study showed a significant increase in developing a first myocardial infarction in periodontitis patients compared to controls[87].

Several hypotheses have been suggested to describe the mechanism of this association[88]. One hypothesis suggests that the local inflammatory response to periodontal pathogens elicits a systemic inflammatory response and hence increases the incidence or worsens existing CVD[88]. In periodontitis patients, inflammatory markers of oxidative stress, including C-reactive protein (CRP) and IL-6, have been found to be elevated systemically[89,90]. These mediators are known to have important roles in the progression of atherosclerosis and CVD[91,92]. In contrast, some studies identified periodontal pathogens, including *Pg and AA,* in atherosclerotic plaque[93]. This

observation suggests that periodontitis could directly enhance atheroma formation through bacteraemia.

Given the association between periodontal disease and CVD, the logical question that follows is, what is the effect of treatment of periodontal disease on the risk of CVD? As mentioned earlier, treatment of periodontitis aims to eliminate or reduce periodontal pathogens through scaling and root planning[38-42]. Faced by the same difficulties in accurately identifying periodontitis, the dynamic nature of the disease renders accurately identifying treatment endpoint quiet challenging. This inherent challenge, partially explains the inconsistent and contradictive results of various studies examining the effect of treatment of periodontitis on CVD. In 2012, Lopez concluded that reducing periodontal inflammation through scaling and root planning was associated with a decrease in CRP levels, a biomarker of CVD[94]. In contrast, in a retrospective cohort study, it was shown that surgical and non-surgical periodontal therapy significantly decreased the incidence of myocardial infarction but had no effect on incidence of stroke[95]. However, in the Periodontitis and Vascular Events (PAVE) study, scaling and root planning resulted in better periodontal clinical parameters but failed to decrease cardiovascular adverse events, compared to non-treatment group[96,97]. In an attempt to overcome the challenge of identifying clinical endpoints of treatment, studies examined edentulous patients, whom by virtue of loss of all teeth, are free of periodontal disease. Importantly, periodontitis is the leading cause of tooth loss in adults[98,99]. In 2001, a study that analyzed the First National Health and Nutrition Examination Survey (NHANES)-1 data showed that extracting all teeth of periodontitis patients did not decrease the incidence or the severity of coronary heart disease events, even after 17 years of edentulism[100]. In contrast, edentulism of periodontitis patients was associated with decreased adverse events and mortality rate in a study analysing cerebrovascular disease and

non-haemorrhagic stroke risk, however, the incident risk was sustained higher than periodontally-healthy controls[101]. Altogether, these studies show an association between periodontal disease and CVD adverse events, and strongly suggest that the periodontitis-induced elevated risk is at least partially sustained after confirmed elimination of the disease clinically.

This phenomenon of sustained effects after disease control or elimination of a risk factor is not seen only in periodontitis. The concept of metabolic memory in diabetes mellitus is a pertinent example. Metabolic memory refers to the sustained beneficial effects of immediate intensive treatment of hyperglycemia, or the sustained detrimental effects of transient hyperglycemia, regardless of the glycemic control in the later course of the disease[102,103]. One hypothesis proposes that prolonged exposure to reactive nitrogen and oxygen species as a result of hyperglycemia, influences downstream biological processes by covalently altering proteins, nucleic acids, and/or lipoproteins, ultimately leading to irreversible degradation[104,105]. In the last 2 decades there has been an interest in understanding this concept of retained memory and more studies are pointing to epigenetics[106,107].

Epigenetics: DNA Methylation

The linguistic translation of the term “epigenetics” is above or on top of genetics. It refers to a set of features and modifications occurring around the genetic sequence that direct and control gene expression without altering the genetic sequence. In other words, epigenetic modifications, through controlling gene expression, change the phenotype but not the genotype. Importantly, these modifications are heritable and dynamic. They occur physiologically during embryonic development and during cell differentiation but and are as well influenced by life style, social habits, nutrition and disease state. Epigenetic modifications control gene expression

by impacting the accessibility to DNA. DNA methylation, one of the well-studied epigenetic modifications, controls gene expression through adding methyl groups to carbon-5 of the cytosine nucleotide in the cytosine-guanine (CpG) islands at the promoter regions, hence hindering binding of transcription factors to the promoters, and inhibiting or decreasing transcription, and vice versa[108] (Figure 1). So, hypomethylation of cytosine nucleotides in the promoter CpG islands is associated with gene expression, whereas hypermethylation is associated with gene silencing[108]. DNA methylation is a tightly-regulated dynamic process, where the level of methylation is the result of two opposing processes, one which adds methyl groups and another that removes them[109,110]. DNA methyltransferases (DNMT) are a family of enzymes that catalyse the transfer of a methyl group to a cytosine nucleotide. DNMT1, DNMT2, DNMT3A, DNMT3B and DNMT3L, are the five members of the family[109]. DNMT1 and DNMT3 represent the foundation for the establishment and maintenance of the methylation state[109]. DNMT3 is a "de novo" enzyme that catalyzes the methylation of unmethylated DNA[111]. On the other hand, and through its selectivity of symmetrical CpG sites, DNMT1 maintains the methylation status, which in turn ensures the heritability of the methylation patterns[112]. *S*-adenosylmethionine (SAM) is the universal methyl group donor[109]. DNMTs transfer the methyl group from SAM to carbon-5 of the cytosine ring[113] (Figure 1). The opposing process, DNA demethylation, is carried out by another family of enzymes, Ten-Eleven Translocase (TET). TET1, TET2 and TET3 constitute this family[110]. TET catalyzes the oxidation of the methylated cytosine (5mc) to 5-hydroxymethylcytosine (5hmC), which is a critical intermediate in the conversion of 5mc to unmethylated cytosine[110]. This dynamic interplay between DNMTs and TETs allows for the needed flexibility and plasticity of genes to respond to different stimuli with the proper transcription order. This is evident in several diseases and pathological conditions. As

mentioned earlier, studies are pointing towards epigenetics changes in inflammatory genes to underlie the metabolic memory phenomenon observed in diabetes mellitus[106,107]. Several studies have looked into a potential role of epigenetics in the pathophysiology of periodontitis. In 2012, Ishida *et al*. found that hypomethylation in the promoter of IL-6 was associated with increased IL-6 serum levels in periodontitis patients[114], suggesting a role for DNA methylation. Similarly, in 2010, Zhang *et al.* found a significant association between hypomethylation in the promoter region of the interferon-gamma gene and its over expression in chronic periodontitis patients compared to healthy controls[115]. In a study that used *Pg* to induce periodontal disease in mice, the authors showed that *Pg*-induced periodontal disease was associated with hypermethylation of the Toll-like receptor (TLR)-2 promoter and blunted gene expression in gingival epithelial cells[116]. In contrast, studies on atherosclerosis and CVD are as well strongly suggestive of a role for DNA methylation in the pathophysiology. Hypomethylation of the IL-6 promoter has been repeatedly associated with overexpression of IL-6 and increased risk of coronary heart disease and myocardial infarction[117,118]. Using apolipoprotein E knock-out ($ApoE^{-/-}$) mice, a well-established atherosclerotic mouse model, differences in DNA methylation were evident and preceded the presence of detectable atherosclerotic lesions[119]. Furthermore, high fat diet feeding of $ApoE^{-/-}$ mice, induced hypomethylation of CpG islands in genes encoding Pu.1 (a transcription factor) and interferon regulatory factor -8, key regulators of monocyte proliferation and macrophage differentiation, and this was associated with a significant increase in monocytes[120].

Figure 1: Cytosine methylation and gene regulation.
A) In the absence of Cytosine methylation in the CpG islands, transcription factors (TF) can bind to the promotor and initiate gene transcription.
B) In the presence of Cytosine methylation (•), binding of transcription factors (TF) to the promotor is hindered and hence gene transcription is attenuated or completely stopped.
C) In the presence of methionine Adenosyltransferase (MAT), methionine, an essential amino acid, is converted to the universal methyl donor, S-Adenosyl methionine (SAM). DNA methyltransferase (DNMT) transfers the methyl group (CH_3) from SAM to the 5-position of cytosine, converting Cytosine to 5-methylcytosine.

A relatively recent concept, referred to as "trained immunity", suggests that innate immune cells can be programmed to develop a different phenotype through exposure to a certain stimulus[121,122]. Monocytes isolated from Bacille Calmette-Guerin vaccinated individuals produced significantly more pro-inflammatory cytokines in response to unrelated microbial metabolites compared to monocytes from non-vaccinated subjects; this was evident even 3 months after vaccination[123]. In the same context, several studies show that pre-exposure of macrophages to certain stimuli, such as LPS or ox-LDL, polarized these cells to a more pro-inflammatory M1 phenotype. This manifested as over production of inflammatory cytokines as well as foam cell formation[124,125]. Importantly, this long-term effect was associated with epigenetic modifications[124].

Atherosclerosis Mouse Model:

The fact that cholesterol and triglycerides are hydrophobic, necessitates their association with lipoproteins for transportation[126]. There are five types of lipoproteins, namely,

chylomicrons, the very low-density lipoprotein (VLDL), low-density lipoprotein (LDL), intermediate density lipoprotein (IDL) and high-density lipoprotein (HDL)[126]. They all contain, in some combination, cholesterol, cholesterol ester, phospholipids, triglycerides and proteins. In the exogenous pathway, dietary cholesterol is metabolised primarily in the intestine via the association with chylomicrons, whereas in the endogenous pathway, VLDL packages triglycerides and cholesterol ester into a phospholipid shell containing apolipoprotein B, to be secreted into the circulation[126]. Lipoprotein lipases in extra hepatic tissues hydrolyze fatty acid-containing triglycerides, converting VLDL to IDL. IDL is either removed from the circulation by the liver LDL receptor (LDLR) or further hydrolysed to LDL, the lipoprotein with highest content of cholesterol[126]. The majority of LDL is cleared form the circulation by liver LDLR and the remining is taken up by extrahepatic tissues such as muscle, heart and adipose tissue[126]. Wild type mice do not develop atherosclerosis even when fed a high fat diet (HFD)[127], and hence studying atherosclerosis in mice requires genetic modification. In one model, apolipoprotein E (Apo E) is knocked out, which allows for accumulation and oxidation of chylomicron remnants, and hence development of atherosclerosis. Another well-established atherosclerosis mouse model was developed through knocking out the LDLR. In this model, the absence of the LDLR allows for accumulation of LDL, raising the plasma cholesterol from 50-80 mg/dL in wild type mice to 200-300 mg/dL[128]. However, this increased cholesterol level is not sufficient to develop atherosclerosis, necessitating feeding these mice a HFD which increases the plasma cholesterol levels to 2000 mg/dL[128]. This is the mouse model we used for this study.

Hypothesis and Objective

Identifying periodontal disease as an independent risk factor for CVD is alarming and warrants extensive research to understand the mechanisms underlying this association.

Importantly, and as mentioned earlier, conventional treatment of periodontal disease through scaling and root planning or even complete teeth extraction does not seem to reverse the increased risk of cardiovascular events induced by periodontal disease. Considering the fact that the longest turnover of immune cells occurs in 120 days[129], this apparent long-term effect points to cells with longer longevity and/or with self-renewing ability. Importantly, this long-term effect also points to changes that can be preserved or passed as cells divide and replicate. In the light of this, we hypothesize that periodontal disease induces epigenetic changes in the form of DNA methylation in the self-renewing hematopoietic stem cells in the bone marrow, and these changes render macrophages more pro-atherogenic.

Our objective was to test this hypothesis through sequential pre-determined aims, using the low-density lipoprotein receptor Knock out (*LDLR*$^{-/-}$) mouse. All mice were fed a high fat diet to induce atherosclerosis, and were either inoculated by *Pg* oral lavage to induce periodontal disease, or sham inoculated, creating to groups of mice that were the donors. After 16 weeks, donor mice were sacrificed and their bone marrow was isolated and transplanted into irradiated gender-matched naïve *LDLR*$^{-/-}$) ^{mice}, creating 2 groups of recipient mice. Group A: mice were recipients of bone marrow from *Pg*-inoculated donors and Group B mice were recipients of bone marrow from sham-inoculated donors. 4 weeks later, all recipient mice were fed a high-fat diet for 16 weeks and then sacrificed. Since all recipient mice were not *Pg*-inoculated, Group A mice that received bone marrow from *Pg*-inoculated donors, theoretically mimic clinical eradication of periodontal pathogens in periodontitis patients, whereas Group B mice that received bone marrow from sham-inoculated donors, mimic periodontally healthy patients. Transplanting the bone marrow from *Pg*-inoculated donors into healthy mice, would enable us to study our hypothesized effect of periodontal disease on hematopoietic stem cells. In the recipient mice we

analysed and compared the atherosclerotic lesions in the aorta, macrophage and plasma cytokine profile, whole genome DNA methylations levels, and activity of DNMTs and TETs. Associations between differences in methylation and/or demethylation activities and DNA methylation levels, as well as associations between the inflammatory profile and atherosclerotic lesion burden could represent a proof of concept of our novel hypothesis as well as identify specific mechanisms underlying the long-term association between atherosclerotic CVD and periodontitis.

CHAPTER 2

Materials & Methods

Materials:

Unless specified otherwise, all reagents, miscellaneous laboratory chemicals, equipment and plasticware were from Fisher Scientific.

Cell Media Recipes

Iscove's Modified Dulbecco's Complete Media

- Iscove's Modified Dulbecco's Media (IMDM, ThermoFisher Scientific - #12440053)
- 10% heat inactivated (55°C waterbath for 2 hours) fetal bovine serum (FBS; Hyclone - SH 30396.03)
- 100 U/mL penicillin and 100 μg/mL streptomycin (Hyclone – SV30010).

Bone Marrow Transplant Media

- IMDM
- 100 U/mL penicillin and 100 μg/mL streptomycin

Dulbecco's Modified Eagle Media (DMEM) L929 Growth Media

- DMEM (Hyclone – SH 30081.01)
- 10% heat inactivated FBS
- 100 U/mL penicillin and 100 μg/mL streptomycin
- 2 mM/L-glutamine (Sigma – G7513)

Bone Marrow Resuscitation Media

- Roswell Park Memorial Institute (RPMI) 1640 (Hyclone – SH 30255.01)
- 10% heat inactivated FBS
- 100 U/mL penicillin and 100 μg/mL streptomycin

- 2 mM/L-glutamine

Bone Marrow Derived Macrophages (BMDM) Differentiation Media

- RPMI 1640
- 10% heat inactivated FBS
- 100 U/mL penicillin and 100 µg/mL streptomycin
- 2 mM/L-glutamine
- 15% L929 Conditioned Cell Media (LCCM)

Mice

We used the *LDLR*$^{-/-}$ mouse strain from Jackson Laboratories (Strain #002207; B6.129S7-*Ldlr*^{tm1Her}/J), a well-established atherosclerosis model, that develops atherosclerotic lesions when fed a high fat diet (HFD) (Teklad 88317 (Envigo), 21% fat, 0.15% cholesterol, no cholate, irradiated)[130-132]. Mice were bred homozygous and we verified the genotype by polymerase chain reaction (PCR). Mice ear notches were digested in 200 µl of 0.01M ethylenediaminetetraacetic acid (EDTA), 1% sodium dodecyl sulfate (SDS), 0.05M Tris, pH 7.5 and 200 ng/ml of proteinase K (Sigma Aldrich – 39450-01-6) in a 55°C water bath, overnight. Sequential equal volumes of tris saturated phenol (Fisher BioReagents - 108-95-2) and chloroform (Fisher Chemical - 67-66-3) were used to separate nucleic acids from protein and other tissue constituents. DNA was precipitated with 2 volumes of 100% ethanol. The DNA pellet was air dried and resuspended in sterile Tris-EDTA + RNase (1M Tris, pH 8, 0.5M EDTA + 4 ug/ml RNase).

Primers for LDLR PCR:

- Common: TAT GCA TCC CCA GTC TTT GG
- Wild Type (WT) Reverse: CTA CCC AAC CAG CCC CTT AC
- Mutant Reverse: ATA GAT TCG CCC TTG TGT CC

Temperature, ^{o}C	Time
95	1 minute
95	30 seconds
53.5	30 Seconds
72	30 seconds
Repeat steps 2-4	39 cylces
72	1 minute
4	Hold

Expected Sizes:

Mutant = ~179 base pairs (bp)

Heterozygote = ~179 bp and 351 bp

WT = 351 bp

We resolved the PCR products on a 1.5% agarose (Fisher BioReagents - 9012-36-6) gel with 0.85 μM ethidium bromide (ThermoFisher Scientific – BP1302 – 10) for visualization. We used Tris-borate- EDTA (TBE) as the running buffer (0.089M Tris, 0.089M Boric acid, 0.002M EDTA). Depending on gel size, percent of agarose was calculated per total gel volume and was added to TBE, heated to boiling point, then allowed to cool and solidify in the gel tray. Molecular weight was determined using GeneRuler 1 kilobase (kb) DNA ladder (ThermoScientific – SM1331). Gel images were taken under ultraviolet illumination using ChemiDoc Imaging system (ChemiDoc MP Imaging System, version 4.1, Bio-Rad).

Experiments and procedures were approved by the University of Alberta Animal Care and Use Committee under animal use protocol # 0570 (Febbraio). The University of Alberta Health Sciences Laboratory Animal Services housed and cared for all mice.

The number of mice was based on a power calculation using this website (http://www.statisticalsolutions.net/pss_calc.php), based on a previous experiment in our lab where sham-inoclulated *LDLR*$^{-/-}$ mice developed 6% mean lesion area and *Pg*-incoultaed LDLR$^{-/-}$ mice developed 12% mean lesion area, with a standard deviation of 6%. Our power calculation indicates the sample size to be 11, for 90% power at a p value $\leq$0.05. Experiments were performed in both sexes as we couldn't have anticipated a different response between sexes before running the experiment.

Atherosclerosis Induction

In donors, atherosclerosis was induced in 4-week-old *LDLR*$^{-/-}$ mice by feeding them the HFD for 16 weeks. In recipient mice, atherosclerosis was induced 4 weeks after bone marrow transplantation, by feeding *LDLR*$^{-/-}$ mice the HFD for 16-20 weeks.

Periodontal Disease Induction

Periodontal disease induction was done similarly to previously published protocols[130,133]. *Pg,* (American Type Culture Collection (ATCC) strain# 33277) was grown for 24-48 hours in Schaedler's broth (Oxoid - CM0497) supplemented with 1% Vitamin K_1 + Hemin (BD Bioscience - 212354) in anaerobic conditions (Mitsubishi AnaeroPack™ 2.5 L anaerobe jar, ThermoScientific - R685025; AnaeroPack™ - Anaero Anaerobic Gas Generator, ThermoScientific - R681001). Saturated cultures were then centrifuged @ 20,000 x *g*. Periodontal disease was induced through oral inoculation by *Pg* oral lavage. The lavage was

prepared by resuspending ~2 x 10^9 colony forming units/mL *Pg* in 2% sterile carboxymethylcellulose (Sigma-Aldrich - 900432), a thickener that improves bacterial adhesion. Using micro applicator brushes (Shintop – X001D3SXEJ) the lavage (200ul/mouse) was applied every other day for 14 days, around the molars on mice gingiva. Control mice were sham inoculated with the vehicle. Prior to inoculation, mice were anesthetized using intraperitoneal (IP) ketamine/xylazine (100 mg/kg ketamine and 10 mg/kg xylazine in a volume of 100 ul). Inoculation started on the same day as the HFD, and mice were housed in a biocontainment facility.

Bone Marrow Donors

At the end of 16-20-weeks HFD feeding, donor mice were euthanized with IP injection of pentobarbital: 200 mg/kg (BiMeda-MTC Animal Health Inc, 00141704), creating two donor groups: *Pg*-donors, and sham-donors, that were inoculated with *Pg* or inoculated with vehicle only, respectively.

Bone Marrow Recipients

12-week-old irradiated *LDLR*$^{-/-}$ mice were transplanted with bone marrow from sex-matched *Pg* or sham donors., forming two groups of recipients.

Group A: recipient mice of bone marrow from donors fed the HFD and inoculated with *Pg*

Group B: recipient mice of bone marrow from donors fed the HFD and sham inoculated (Figure 2)

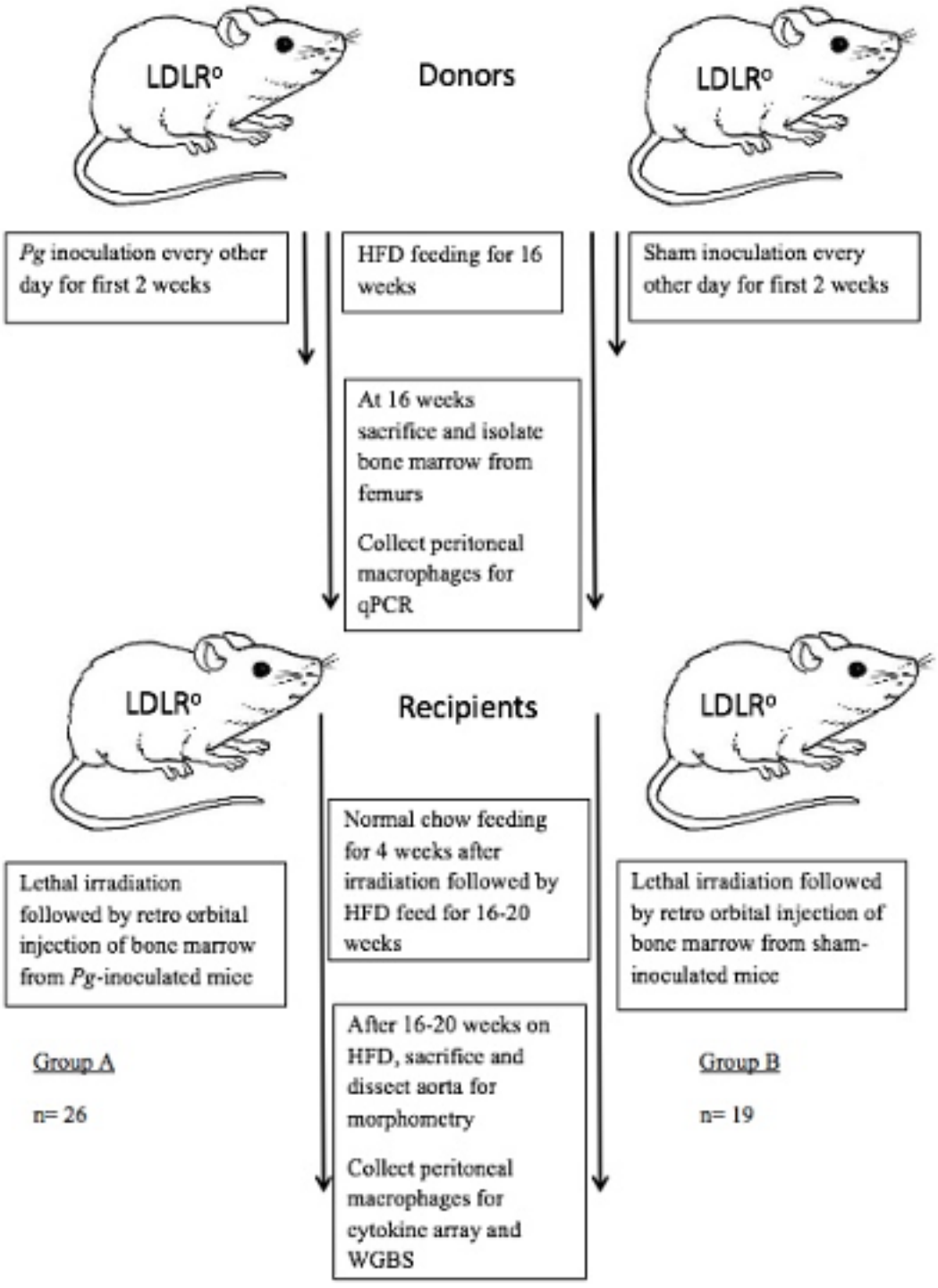
LDLR⁰
Donors
LDLR⁰
Pg inoculation every other day for first 2 weeks
HFD feeding for 16 weeks
Sham inoculation every other day for first 2 weeks
At 16 weeks sacrifice and isolate bone marrow from femurs
Collect peritoneal macrophages for qPCR
LDLR⁰
Recipients
LDLR⁰
Lethal irradiation followed by retro orbital injection of bone marrow from *Pg*-inoculated mice
Normal chow feeding for 4 weeks after irradiation followed by HFD feed for 16-20 weeks
Lethal irradiation followed by retro orbital injection of bone marrow from sham-inoculated mice
After 16-20 weeks on HFD, sacrifice and dissect aorta for morphometry
Collect peritoneal macrophages for cytokine array and WGBS
Group A
n= 26
Group B
n= 19

Figure 2: Study Design
Donor LDLR$^{-/-}$ mice were fed HFD for 16 weeks to induce atherosclerosis, and for the first 2 weeks were either inoculated orally with *Pg* to induce periodontal disease or sham inoculated. At the end of the 16 weeks, mice were sacrificed and bone marrow was isolated. Peritoneal macrophages were collected for RT-qPCR. Recipient LDLR$^{-/-}$ mice were lethally irradiated to ablate their native bone marrow, then were transplanted with bone from *Pg*-inoculated donors (Group A) or from sham-inoculated donors (Group B). Recipient mice were fed normal chow for 4 weeks after transplant then were fed HFD for 16-20 weeks, before they were sacrificed. At time of sacrifice, the aorta was dissected to perform aorta morphometry and determine lesion burden. Peritoneal macrophages and plasma were as well collected for cytokine array and WGBS.
LDLR$^{-/-}$: Low Density Lipoprotein Receptor Knock-out, HFD: High Fat Diet, RT-qPCR: Quantitative Polymerase Chain Reaction, Pg: Porphyromonas gingivalis, WGBS: Whole Genome Bisulphite Sequencing

Irradiation Protocol

The dose necessary to eradicate bone marrow stem cells was 11 Gray (Gy). Similar to a previously published protocol[134], mice were irradiated using a split dose protocol, 2 x 5.5 Gy, using a Cesium-137 source (Gammacell 1000 Elite irradiator, Alberta Diabetes Institute Core Facility). We determined the time needed to generate 5.5 Gy using this formula:

$$T = \frac{Desired\ Central\ Dose\ (Gy)}{\left(Central\ Dose\ Rate\ [\frac{Gy}{min}]\right) * Decay\ Factor}$$

Central dose rate was defined as 11.53 Gy/minute. The decay factor is a function of the Cesium-137 half-life and therefore the value changed based on the date of transplant. Once calculated, 5.5 Gy was given twice, 4 hours apart, then mice rested for 2 hours before transplantation.

Bone Marrow Transplantation

Sham and *Pg* donor mice were euthanized by IP injection of pentobarbital at a dose of 200 mg/kg (BiMeda-MTC Animal Health Inc, 00141704). Limbs were excised, and cleaned of skin,

muscle, and connective tissue. The tibia and femur were excised and cleaned of skin, muscle and connective tissue as much as possible then detached at the knee joint, to be processed separately. Using a 1 ml syringe and 25-gauge needle, the bone was pierced at either end and marrow was flushed repeatedly with complete Iscove's Modified Dulbecco's Media (IMDM). Cells (~2 x 10^7/donor mouse) were centrifuged for 5 minutes at 3783 x *g*, and resuspended at a concentration of ~10^7 cells/mL in bone marrow transplant media. Bone marrow cells (~5 x 10^6 donor cells/mouse) were transplanted through retro-orbital injection. Bone marrow cells from 1 mouse were transplanted into 4-5 recipient mice. Following transplant, recipient mice were housed in sterile caging with autoclaved water and fed a standard chow diet for 4 weeks to allow for full engraftment and hematopoietic cell turnover, followed by the HFD for 16-20 weeks.

Irradiation and Transplant Efficacy Control

As a control for our transplant procedure, we used five $CD36^{-/-}$ mice. $CD36^{-/-}$ mice were irradiated at the same time as $LDLR^{-/-}$ mice, and subsequently transplanted with CD36 WT bone marrow. We isolated DNA from peripheral blood and applied a PCR assay to identify the subsequent genotype 4 weeks later, which allows for full turnover of hematopoietic cells and engraftment of donor stem cells in recipient animals.

Primers for CD36 PCR:

Common: CAGCTCATACATTGCTGTTTATGCATG

WT: GGTACAATCACAGTGTTTTCTACGTGG

Mutant: CCGCTTCCTCGTGCTTTACGGTATC

Expected Sizes:

Mutant = ~800 bp

WT = 600 bp

Temperature, °C	Time
94	2 minutes
94	1 minute
65	1 minute
70	2 minutes
Repeat steps 2-4	30 cycles
72	
4	hold

Plasma Collection

Prior to plasma collection, recipient mice were starved overnight for 16-18 hours. Mice were euthanized with a 200 mg/kg pentobarbital IP injection. 1 mL of blood was collected through heart puncture, in an EDTA-coated 1 ml syringe. EDTA was added to a final concentration of 5 mM. To separate erythrocytes and leukocytes from plasma, whole blood was centrifuged for 5 minutes at 3783 x g. Plasma was removed, aliquoted, and stored at -20°C.

Peritoneal Macrophages

Four days before euthanasia, macrophages were elicited from donor and recipient mice by injecting mice IP with 2 ml sterile 4% Brewer's thioglycolate media. After euthanasia with pentobarbital IP injection, macrophages were harvested by peritoneal lavage into sterile phosphate-buffered saline (PBS). Cells were centrifuged (5 minutes @ 870 x *g*) and pelleted, then frozen at -20°C in anticipation of DNA isolation.

DNA Isolation from Peritoneal Macrophages

First, macrophages were incubated in 1% SDS and proteinase K at 55°C overnight, then vortexed. 200 ul of tris-saturated phenol was then added to the lysate and vortexed, followed by

centrifugation for 5 minutes at 21913 x *g.* The aqueous layer (top) was then removed to a new tube and a 200 ul of chloroform (Fisher Chemical - 67-66-3) was added, vortexed and then centrifuged for 5 minutes at 21913 x *g*. The aqueous layer (top) was then removed to a new tube. By slowly dripping 2 volumes of 100% ethanol, DNA was brought out of solution, followed by 5 minutes centrifugation at 21913 x *g*. The supernatant was removed and the DNA pellet was air dried and then resuspended in sterile Tris-EDTA + RNase (1M Tris, Ph 8, 0.5M EDTA + 4 ug/ml RNase).

RNA Isolation from Donor Peritoneal Macrophages

RNA was purified from peritoneal macrophages using the RNeasy Mini Kit by Qiagen, following their protocol. Briefly, cells were incubated with the kit lysis/binding buffer and one volume of 70% ethanol was added. The lysate with the ethanol was transferred to a spin column placed in a 2 ml collection tube. The ethanol and binding buffer facilitated RNA and DNA binding to the silica membrane, so that when the lysate was centrifuged for 15 seconds at 8000 x g, the contaminating cellular components were collected in the collection tube and discarded. 80 ul of kit included RNase-free DNase solution were then added to the membrane for 15 minutes and then centrifuged for 15 seconds at 8000 x g. The DNA was hence collected in the collection tube and discarded. This was followed by three washes with kit-provided washing buffer and then finally RNA was eluted in 30 ul RNase-free water. RNA was immediately frozen at -80^{o}C.

Complementary DNA (cDNA) Synthesis

cDNA was synthesised from purified RNA using the RT^{2} First Strand Kit by Qiagen, following their protocol. Briefly, 25 ng to 5 µg of RNA were incubated with 14 ul genomic DNA elimination buffer for 5 minutes at 37^{o}C and then incubated with 6 ul of kit provided reverse

transcriptase mix for 15 minutes at 42ºC. The reaction was stopped by heating at 95ºC for 5 minutes. cDNA was used immediately for quantitative PCR (RT-qPCR) or stored at -20ºC.

DNA Quality Control

Agarose gel electrophoresis

Integrity and purity of isolated DNA was assessed using 1% agarose gel electrophoresis. 200 ng of DNA was added to sterile water and 2X DNA loading dye (ThermoFisher Scientific – R0611). DNA and GeneRuler 1 kilobase (kb) DNA ladder were electrophoresed for 30 minutes at 15 milliampere (mA). ChemiDoc™ MP Imaging System and Image Lab 5.0 software, were used to capture and analyse gel images. We made sure that there was no genomic DNA contamination or visible signs of degradation, that would manifest as high molecular weight bands or smear, respectively.

Qubit® Fluorometric Analysis and Nucleic Acid Spectrophotometry**.**

This was done at University of Alberta Faculty of Medicine & Dentistry Applied Genomics Core (TAGC). As requested by Novogene Co. Ltd, Qubit® 2.0 Fluorometer system (ThermoScientific) in conjunction with the Qubit™ dsDNA High-Sensitivity Assay Kit (ThermoScientific – Q32854), were used to quantify isolated DNA concentrations. Briefly, in Axygen PCR-05-C tubes (VWR – 10011-830), 1 µL of isolated DNA was added to 199 µL of a working solution, vortexed and incubated at room temperature for 3 minutes, then read using Qubit® 2.0

RNA Quality Control

Integrity and purity of isolated DNA were assessed using 1% agarose gel electrophoresis. 400-600 ng of RNA were added to 2X RNA loading dye (ThermoFisher Scientific – R0641) and loaded

onto the gel. RNA and GeneRuler 1 kb DNA ladder (ThermoScientific – SM1331) were electrophoresed for 60 minutes at 70V, constant voltage. If the 28S:18S ratio was 2:1, RNA was regarded acceptable in addition to absence of high molecular weight bands suggestive of genomic DNA contamination, or smearing which indicates degradation. In addition, NanoDrop™ was used to further assess purity, using 1 ul of purified RNA and adjusting it to the wavelength reading of the blank solution (RNAse-free water). RNA was considered pure if the ratio A_{260}/A_{280} of was ~ 2. Lower ratios are suggestive of protein contamination.

Aorta Morphometry

Using pentobarbital overdose (200 mg/kg, IP), mice were euthanized, and perfused with 10 ml PBS then vasculature fixed with 5 ml buffered formalin (FormaldeFresh). The complete aorta, including the subclavian, left and right carotid arteries were dissected from the mouse and then post-fixed in buffered formalin at 4°C. Aortae were transferred to PBS after 24 hours and stored at 4°C. Using oil red O (Sigma Aldrich – 1320-06-05), which identifies neutral lipids in plaque, aortas were stained for 30 minutes followed by 1-2 minutes of de-staining with methanol. Each aorta was placed open on a microscope slide, covered with a coverslip, and hydrated in PBS, and digitally scanned, using the CanoScan LiDE 210 scanner at 1200 dpi and depth of 24 bit. Using Adobe Photoshop software, three independent measures of lesion area (red pixels) were chosen and averaged for each aorta. Likewise, the total aorta area was calculated. The lesion area was represented as a mean percent of the total aortic area.

qPCR

cDNA synthesized from donors' peritoneal macrophages' RNA was used in this experiment. This assay in in compliance with the Minimum Information for publication of Quantitative real-

time PCR Experiments (MIQE) guidelines. We analysed the gene expression of IL-1β and IL-6 and we used glyceraldehyde 3-phosphate dehydrogenase (GAPDH) as a housekeeping gene. Primers and positive control templates were *Bio-Rad PrimePCR™ PreAmp for SYBR Green Assay* and *PrimePCR™ Template for SYBR Green Assay*, for the respective genes (IL-1β – ID qMmuCED0045755, IL-6 – ID qMmuCED0045760, GAPDH – ID qMmuCED0027497). All samples were run in triplicates. In a 96-well plate, each well constituted of 1 ul of 20x PrimerPCR assay, 10 ul of 2x SsoAdvanced universal SYBR Green supermix (Bio-Rad – 1725271), 4 ul of cDNA sample, and 5 ul of nuclease-free water. We ran a positive control using the respective template and a negative control. Data was analysed using CFX MAnager™

To determine the ideal housekeeping gene, we used *Reference Gene M96* (Bio-Rad), a predesigned 96-well panel preplated with 14 commonly used housekeeping genes. We ran the 2 samples from the donor mice in triplicates for each gene, and the most stable gene under our experimental conditions, GAPDH, was therefore selected to be our housekeeping gene.

We used the following protocol:

Temperature °C	**Time**
95	1 minute
95	5 seconds
60	30 seconds
Repeat steps 2 and 3	40 cycles
Melt Curve 65-95 (0.5 increments)	5 seconds/increment

We used C1000 Touch™ Thermal Cycler (CFX96™ Real-Time System) by Bio-Rad.

Cytokine Array

Macrophage and plasma cytokine profiles were assessed using the Mouse Cytokine Array Panel A (R&D Systems- ARY006), following their recommended protocol. Samples from 5 mice per group were pooled together. For this assay, nitrocellulose membranes coated with duplicates of 42 capture antibodies were used. Dilutions of 10-weeks-old mice plasma from recipient mice, or peritoneal macrophage lysates (macrophages collected at time of sacrifice), were incubated for 1 hour with a cocktail of biotinylated detecting antibodies. At the same time the membranes were incubated with a blocking solution for 1 hour. Following that, the sample/antibody combination was incubated with the blocked membrane overnight at 2-8^{o}C. Any cytokine/detection antibody combination present on the membrane would be bound by its corresponding immobilised capture antibody. Streptavidin- Horseradish peroxidase (HRP) and chemiluminescent detection reagents were applied sequentially after washing with kit-provided 1X wash buffer to remove unbound protein. Each spot produces light in accordance to the amount of cytokine bound. ChemiDoc™ MP Imaging System and Image Lab 5.0 software were used to capture and analyse the image. The average density of the duplicate spots representing each cytokine was determined, then the density of the negative control spot was subtracted from that value. Corresponding values on different membranes were compared to determine the difference between samples.

Whole Genome Bisulphite Sequencing (WGBS)

Novogene Co. Ltd performed all sequencing, library construction, analysis and quality control (https://en.novogene.com/next-generation-sequencing-services/gene-regulation/whole-genome-bisulfite-sequencing/). Below is a summary of their procedures (Figure 3).

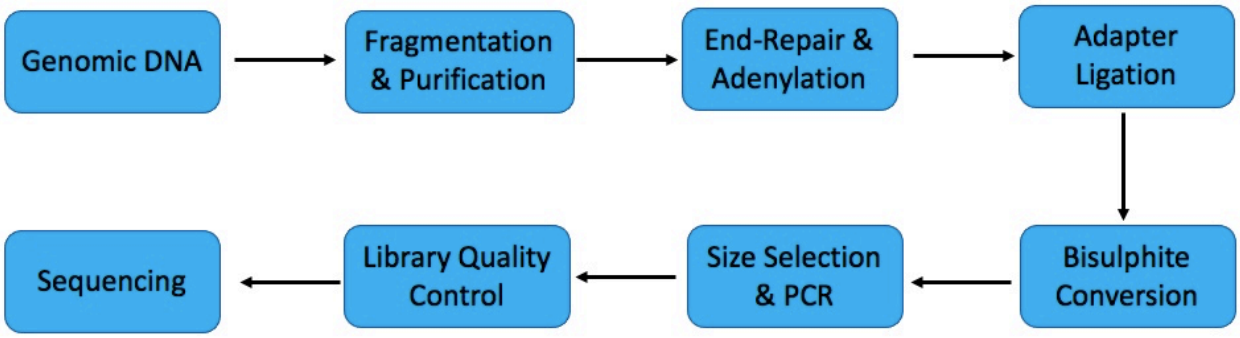

Figure 3: Steps for Whole Genome Bisulphite Sequencing
Genomic DNA purified from recipient mice peritoneal macrophages was prepared by us and sent to Novogene Co. Ltd. DNA was then fragmented into 200-300 base pair fragments. Adenine was then added to the fragments followed by ligation with Thymine. DNA was then treated with bisulphite, which converts unmethylated cytosine to uracil. DNA library was completed by amplifying the fragments via PCR. Sequencing was done using Paired-end sequencing.

Library Construction:

Following the verification of DNA quality, negative control DNAs were added to the DNAs, which were then fragmented into 200-300 bp using the ultrasonicator, Covaris S220. Following that, the DNA fragments were subjected to terminal repairing by addition of adenine, followed by thymine-adaptor ligation. This was followed by bisulphite treatment using EZ DNA Methylation Gold Kit, (Zymo Research). In turn, unmethylated cytosine were converted into uracil, while methylated cytosines were unchanged. 200-300bp fragments were then amplified using PCR. At that point, the final DNA library was ready.

Library quality control:

The library concentration was initially determined using Qubit2.0, then diluted to 1 ng/ul before being checked for insert size on an Agilent 2100 and finally measured with more precision using qPCR (effective library concentration >2 nM).

Sequencing:

Following successful library testing, libraries of each group were combined and fed into HiSeq devices according to effective concentration and predicted data volume. Paired-end sequencing is the method used for sequencing.

Raw Data Quality Control and Trimming:

Base calling transforms the original images obtained from high-through sequencing systems (e.g., Illumina HiSeq™) into sequencing reads, which are referred to as raw data or raw reads and saved in fastq format files. These files contain read information as well as information on sequencing quality.

Raw reads were trimmed to filter out contaminated adaptor sequences and low-quality reads in order to produce qualified clean data. Trimmomatic is a versatile read trimming tool for Illumina NGS data, with the following set of trimming stages and associated parameters.

1) Sliding window: raw reads were scanned in 4 bp increments. Any poor-quality reads were removed.

2) Leading and trailing:3: Removes poor quality bases at the 5' and 3' end of a read

3) Illuminaclip: 2:30:10: Removes adapter and Illumina-specific sequences from the read.

4) Minimum length trimming:36: specifies the minimum read length to be at 36 bp

5) After trimming, the unpaired reads were discarded.

Alignment to Reference Genome:

Bisulphite-treated reads were aligned to a reference genome using the Bismark programme (Krueger, 2011). In sequence reads and the reference genome, C is turned to T and G is transformed

to A (reverse complementary), and then these sequencing reads are aligned to similarly converted versions of the genome separately. The alignment procedure used by Bismark is as follows:

1) Convert both sequencing reads and a reference genome from C to T and G to A.
2) Align converted reads to the converted genome
3) The final result, is the best alignment out of the four parallel alignment processes

Identification of Methylated Cytosines:

Bismark (Krueger, 2011) is used after alignment to identify methylated sites. After removing PCR duplicates, the methylation state of cytosines was determined by comparing the reads base to the reference genome base at the same position. If the read base was C, this cytosine was methylated; otherwise, it was unmethylated.

Determining Methylation Levels:

The methylation level was calculated for methylated sites using the following formula: ML=mC/(mC+umC). The methylation level was represented by ML, and the number of methylated and unmethylated cytosines is represented by mc and umC, respectively.

Identifying Differentially Methylated Regions (DMR):

SwDMR (http://122.228.158.106/swDMR/) is used to detect DMRs in experiments without biological replicates, and is suitable for bisulphite sequencing of two or more samples, including DMR identification, annotation, and visualisation. The software scans the entire genome using a sliding-window approach based on methylation information from each site.

Its workflow primarily consists of:

1) Set the sliding window size (1000 bp) and step length (100 bp), and select regions with methylation level difference values or fold change values greater than the cut-off value, as well as regions with more cytosines than the cut-off value (at least 0.1 methylation level difference and 2 or more fold change, and at least 10 cytosines in the specified region).
2) To perform a significant difference test, the software combined various relevant statistical approaches (Fisher's exact test), and the regions with significant differences were designated possible DMRs.
3) With the provided step length, perform hypothesis testing for the methylation information of the next window.
4) Repeat the methods above several times to obtain probable DMRs across the whole genome.
5) P value was adjusted using False Discovery Rate (FDR) values
6) Merge putative DMRs that overlapped into a single location and run hypothesis testing again. The combined DMR will be used as the final product.
7) When the locations of DMRs and specific genomic functional elements overlap, related genes are chosen and labelled as DMR related genes.

Identifying Differentially Methylated Promotors (DMP):

The promoter region is set to the upstream 2 kb of the Transcription Start Site, (TSS), and its cytosine sites are retrieved. Then, methylation levels are calculated for each cytosine site in the target promoter region as follows: the read numbers that cover cytosine sites in the DMP region and give a methylated count in the sample, divided by all the read numbers that cover cytosine sites in the DMP region in the sample. Then Fisher's exact test is performed for sample A (DNA of recipient mice of bone marrow from donors fed HFD and inoculated with *Pg)* versus sample B

(recipient mice of bone marrow from donors fed HFD and sham inoculated), and the p-value is corrected using FDR to get the p-adjusted (p_{adj}) value The DMP is then filtered so that its p_{adj} is smaller than the cut-off (p_{adj}< 0.05, and methylation level difference more than 0.2)

Generation of Bone Marrow Derived Macrophages (BMDM)

Pentobarbital at a dosage of 200 mg/kg was injected IP into mice to euthanize. The femur and tibia were removed, cleaned, then flushed with complete IMDM. The bone marrow cells were then centrifuged (5 minutes @ 3783 x g) and the pellet resuspended at a concentration of 1 x 10^7 cells per cryovial in a mixture of 90% FBS and 10% dimethyl sulfoxide (DMSO). Each cryovial contained 1 ml of the solution. Cells were stored at -80°C.

BMDM were generated following previously published protocols[135]. To dilute out DMSO, frozen bone marrow cells were resuscitated by gently thawing at 37°C and then transferred to a 15 ml tube. Drops of resuscitation media (9 ml) were dropped along the tube's wall. Cells were centrifuged (5 minutes @ 870 x *g*), and pelleted cells were resuspended in 10 mL BMDM resuscitation media. Cells were plated in 100 mm bacterial plates (2 plates/sample) to allow for easier detachment of cells, and incubated at 37°C in 5% CO_2 atmosphere. On the fourth day following the initial culture, BMDM resuscitation media was removed and 10 mL of BMDM differentiation medium were added to the culture, and macrophages were allowed to develop.

L929 Conditioned Cell Media (LCCM)

We used L929 cells from ATCC (NCTC clone 929 [L cell, L-929, derivative of strain L] (ATCC® CCL-1™)). LCCM was created using DMEM L929 Growth Media. L929 cells were cultivated to near confluency in 10 mL DMEM L929 Growth Media. At day 10, another 10 ml

were added for an additional 10 days. The 20 mL supernatant obtained at day 20 was LCCM. LCCM was sterilized through a 0.2 μm filter, aliquoted and stored at -20°C until needed.

Nuclear Extraction

Nuclear extracts of BMDM were prepared using EpiQuik Nuclear Extraction Kit (Epigentek-OP-0002-1), following their protocol. BMDM differentiation media was removed and cells washed twice with PBS. Cells were detached using 300 ul of 0.25% Trypsin-EDTA (Gibco - 25200-072), then collected and pelleted. Cells were then incubated with a pre-lysis buffer, contained within the kit, on ice for 10 minutes. The combination was then centrifuged for 1 minute at 16099 x *g*, creating a nuclear pellet and supernatant cytoplasmic extract. The cytoplasmic extract was removed and stored at -80ºC. The nuclear pellet was then incubated on ice with kit-provided lysis buffer, protease inhibitor and detergent for 15 minutes with vortexing. The suspension was then centrifuged for 10 minutes at 4ºC at 21913 x *g*. The supernatant nuclear extract was transferred to a new tube and stored at -80ºC. The concentration of the nuclear extract was determined using a bicinchoninic acid (BCA) protein assay.

Protein Assay

To determine the concentration of the nuclear extracts, we used the Pierce™ BCA Assay Kit (ThermoFisher Scientific – #23227) and followed their protocol. Standard samples in the range of 5-250 ug/mL were prepared, using kit-provided albumin. Given the limited amount of nuclear extract, we diluted our nuclear extract sample to be used in this assay in sterile RNAse-free water at 1:10 dilution. In a 96 well plate, in duplicates, 10 ul of the diluted samples, standards and blank were added to 200 ul BCA working reagent, and were mixed on a plate shaker for 30 seconds. The plate was then covered and incubated at 37ºC for 30 minutes. The plate was then

brought to room temperature and then was read on a microplate reader at OD 562 nm. The average OD 562 measurement of the blank was subtracted from the samples and standards measurement. A standard curve was then plotted using the blank-corrected measurements, and the sample protein concentration was determined accordingly.

DNMT Activity Assay

To determine DNMT activity, we used the EpiQuik DNA Methyltransferase Activity/Inhibition Assay Kit (Epigentek- P-3001-2), and followed their protocol. BMDM nuclear extracts were used in this assay. Briefly, in a 96-well plate, samples and controls were incubated with DNMT assay buffer and SAM, the universal methyl donor, for 90 minutes at 37°C. After washing with kit-provided 1X wash buffer, sample and controls were incubated with capture antibody that binds to 5mC for 1 hour at room temperature. After washing with kit-provided 1X wash buffer, samples and control were incubated with detection antibody for 30 minutes at room temperature, then washed with kit-provided 1X wash buffer and developed. The plate was read on a microplate reader at OD 450 nm. DNMT activity was calculated using the following formula:

DNMT activity (OD/h/mg) =

$$\frac{\text{Sample OD} - \text{Blank OD}}{\text{Protein Amount (μg) x 1.5 hours(h)}} \; x \; 1000$$

TET Activity Assay

To determine TET activity, we used the Epigenase™ 5mC-Hydroxylase TET Activity/Inhibition Assay Kit (Epigentek- P-3086-96), and followed their protocol. BMDM nuclear extracts were used in this assay. Briefly, a 96-well plate was first coated with TET substrate by incubating binding solution with TET substrate for 90 minutes at 37°C. Binding solution was then removed

and wells washed with kit-provided 1X wash buffer. Samples and standard control were then incubated with TET assay buffer for 90 minutes at 37°C. After washing, 5hmC capture antibody was added and the plate was incubated for 60 minutes at room temperature. After washing with kit-provided 1X wash buffer, capture antibody against 5hmC was added and the plate was incubated for 30 minutes, then washed using kit-provided 1X wash buffer. Detection solution was then added and the color started to develop. When the color of the standard positive control reached medium blue, stop solution was added to stop the reaction. The plate was read on a microplate reader at OD 450 nm. TET activity was calculated using the following formula:

$$\text{Hydroxymethylated product (ng)} = \frac{\text{Sample OD} - \text{Blank OD}}{\text{Slope}}$$

$$\text{Hydroxymethylated product (ng)} = \frac{\text{Hydroxymethylated product (ng)}}{\text{Protein amount (ug)} x\ 90\ mins}$$

SAM and SAH Plasma Levels

We measured the plasma levels of SAM and S-Adenosylhomocysteine (SAH) using the S-Adenosylmethionine and S-Adenosylhomocysteine ELISA Combo Kit (Cell Biolabs - MET-5151-C), and followed their protocol. At time of sacrifice, plasma from 3 mice/group was collected. Using Magne™ Protein A Beads (Promega, catalog #), IgG was removed from plasma samples prior to measuring SAM and SAH levels. First, the bead slurry was aliquoted to 50 ul in 1.5 ml microcentrifuge tubes. The tubes were then placed in a magnetic stand for 10 seconds and in this way, the storage buffer was removed. The beads were then washed with 500 ul PBS, and the tubes placed in the magnetic stand for 10 seconds and the buffer was removed. 50 ul of wash buffer was then added to 50 ul of plasma, the combined sample was then incubated with the

equilibrated beads for 60 minutes at room temperature in a tube shaker. The tubes were then placed in a magnetic stand for 10 minutes, and the supernatant, being the plasma without IgG, was transferred to a new microcentrifuge tube.

After IgG removal, the wells of a 96-well plate were coated with either SAM or SAH conjugate by incubating it overnight at 4^{o}C. The wells were then blocked using assay diluent for 1 hour at room temperature. Plasma samples and standard controls were added to the coated wells and incubated for 10 minutes on an orbital shaker at room temperature. Anti-SAM or anti-SAH antibodies were then added to the wells and incubated for 1 hour on an orbital shaker at room temperature. After washing with kit-provided 1X wash buffer, a secondary antibody HRP conjugate was added to the wells and incubated again for 1 hour at room temperature. After washing with kit-provided 1X wash buffer, the plate was developed and then read on a microplate reader at OD 450 nm. A no-primary antibody control was included for each sample. The amount of SAM and SAH in the plasma samples was then calculated using the standard curve after accounting for the no primary antibody control.

$$\text{SAM or SAH (nM)} = \frac{(\text{Sample OD} - \text{No Primary Antibody Control OD}) - \text{Blank OD}}{\text{Slope}}$$

DNMT activity, TET activity and SAM and SAH experiments were done on a different mice cohort than used in the atherosclerosis study. In this cohort, the bone marrow recipients were not fed the HFD. In addition, mice were sacrificed one year after bone marrow transplant, and hence, bone marrow cells and plasma were collected one year after bone marrow transplant.

Statistical Analysis

The differences in donors' gene expression, and atherosclerosis lesion burden, DNMT activity, TET activity, and SAM and SAH plasma levels between groups A and B, were statistically compared using an unpaired t-test (if samples passed the D'Agostino & Pearson omnibus normality test) or a Mann-Whitney U analysis, with significance set at $p < 0.05$. GraphPad Prism software was used for all statistical analyses.

CHAPTER 3

Results

Bone marrow irradiation/transplant efficacy: Bone marrow engraftment 4 weeks after transplantation

In this study, donors and recipients are syngeneic *LDLR*$^{-/-}$, therefore it is not possible to directly determine the success of bone marrow ablation. Therefore, we opted to use a control experiment. We recruited CD36$^{-/-}$ mice as a control for our transplantation technique. CD36$^{-/-}$ mice were irradiated coincidentally with a group of *LDLR*$^{-/-}$ mice, and then transplanted with CD36 wild type (WT) bone marrow. 4 weeks later, which allows for lymphohemtopoietic reconstitution of all cell lineages in recipient mice, we purified DNA from peripheral blood and performed a PCR assay to determine subsequent genotype. All 5 recipient mice showed only the CD36 WT genotype, under conditions in which control DNA successfully amplified CD36 WT and CD36$^{-/-}$ alleles (Figure 4).

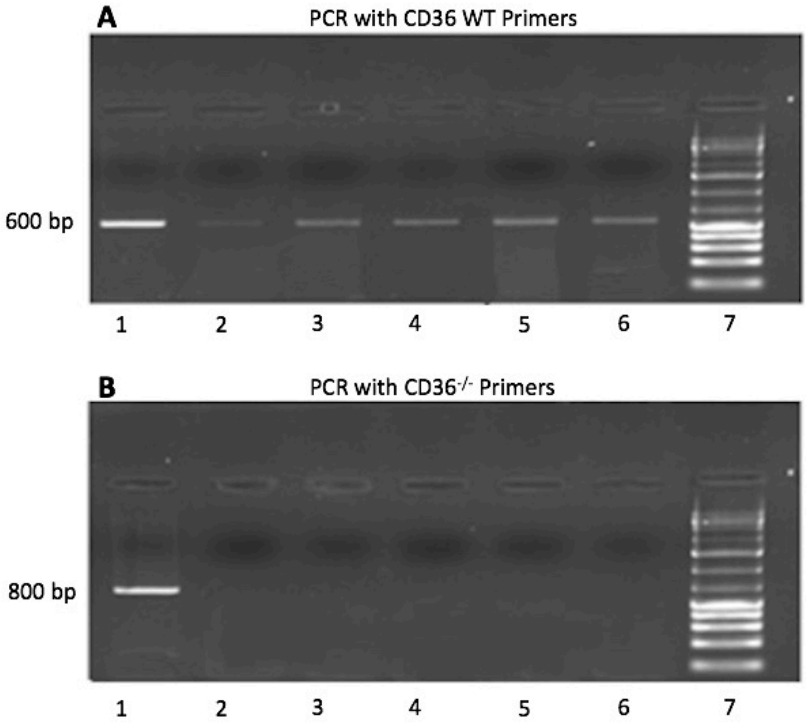

Figure 4: Successful bone marrow engraftment confirms efficacy of the transplantation protocol. CD36$^{-/-}$ mice were lethally irradiated then transplanted with CD36 WT bone marrow. 4 weeks after bone marrow transplant PCR was done using CD36 WT primers (A) and CD36$^{-/-}$ primers (B). On 1% agarose gel, under conditions in which control DNA successfully amplified CD36 WT and CD36$^{-/-}$ alleles, all 5 mice showed bands of 600 bp corresponding to CD36 WT genotype (A), but none showed bands of 800 bp which corresponds to CD36$^{-/-}$ genotype (B). Lane1: Positive control, Lanes 2-6: Experimental mice, Lane 7: 1 kb ladder

In addition, irradiated *LDLR*$^{-/-}$, without BM transplant would succumb to sepsis 2 weeks after irradiation when all hematopoietic cells die. There was 0 mortality in our experiments.

Furthermore, the efficacy of the irradiation protocol was confirmed through flow cytometry. In this experiment we transplanted CD36 WT mice with CD36$^{-/-}$ bone marrow. Monocytes were positively and negatively gated based on CD11b and CD11c respectively (CD11b^{+}/CD11c^{-}), and stained for expression of CD36. Cells from non-transplanted, CD36 WT showed a CD36^{+} monocyte population of 18.6%, whereas, those transplanted with CD36$^{-/-}$ bone marrow, showed less than 1%, in three different transplant recipients (Figure 5). This indicates that our irradiation and transplantation techniques were successful. These irradiation and transplantation conditions were applied to all subsequent *LDLR*$^{-/-}$ mice. This experiment was done by Cole Delyea, a student at Dr. Shokrollah Elahi's lab.

Oral inoculation with *Pg* elicits a systemic inflammatory response in donor mice

To induce periodontal disease, we applied *Pg* by oral lavage to the mice gingival margins around upper and lower teeth, every other day for 2 weeks[119]. A control group of mice were sham inoculated with vehicle. Both groups were fed a HFD for 16 weeks. Using qPCR, we determined the gene expression of the inflammatory markers, IL-1β and IL-6, in thioglycolate-elicited peritoneal macrophages. Both these cytokines are known to be essential to the destructive inflammatory effects of *Pg* infection, and are biomarkers for periodontal disease[50]. As expected, if a successful chronic periodontal disease state had been achieved, there was a significant 2-3-fold increase in expression of both cytokines in macrophages from mice that were inoculated with *Pg* compared to sham inoculated mice (Figure 6).

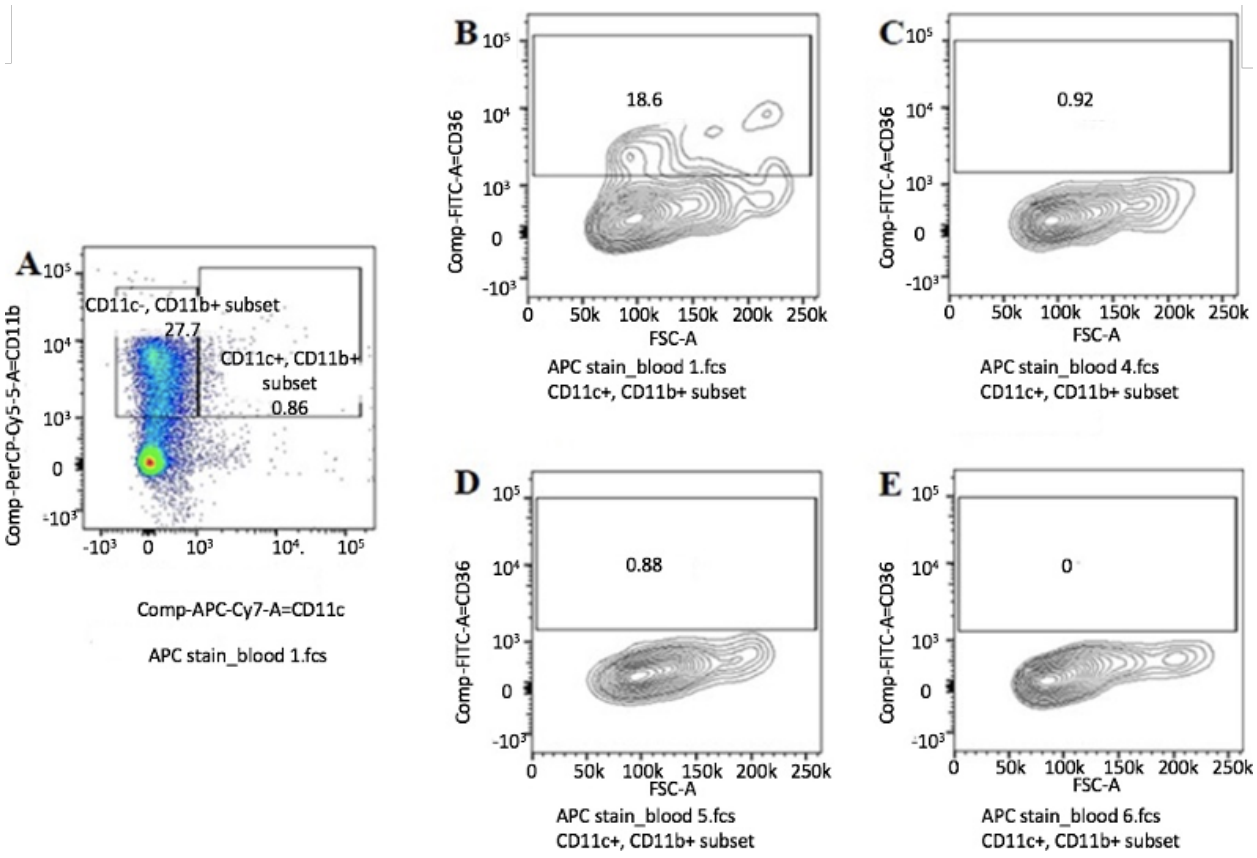

Figure 5: Successful ablation of native bone marrow confirms efficacy of irradiation protocol. CD36 WT mice were irradiated with 2 X 5.5 Gy, and transplanted with $CD36^{-/-}$ bone marrow. 4 weeks later, chimerism was assessed in peripheral blood monocytes. Monocytes were positively and negatively gated based on CD11b and CD11c, and stained for expression of CD36 (A). CD36 expression in control non-irradiated non-transplanted CD36 WT mouse, 18.6% (B). CD36 expression in 3 mice irradiated and transplanted with $CD36^{-/-}$ bone marrow, <1% (C, D, E). This experiment was done by Cole Delyea, a student at Dr. Shokrollah Elahi's lab.

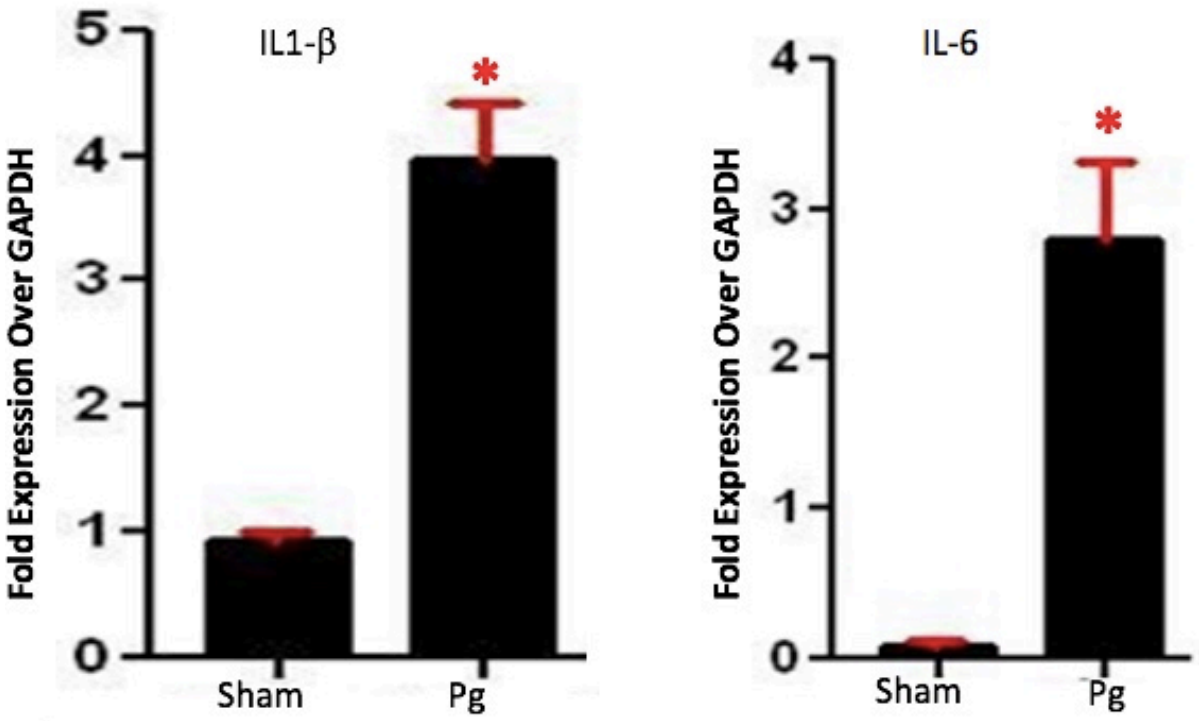

Figure 6: *Pg* elicits an increased inflammatory response in macrophages from donor mice.
Using RT-qPCR, at time of sacrifice in donor mice, we determined the gene expression of the inflammatory markers IL-1β and IL-6, in thioglycolate-elicited peritoneal macrophages. Both genes were expressed significantly more in mice fed the HFD and inoculated with *Pg* (Pg) compared to mice fed the HFD and sham inoculated (Sham). GAPDH was used as the housekeeping gene. * $p < 0.05$

Group A mice have increased atherosclerotic lesion burden compared with Group B mice

After 16 weeks of HFD feeding, all recipient mice were sacrificed and the aorta dissected and stained with oil-red-O[136] (Figure 7A). Using Adobe Photoshop, we performed morphometric analysis to determine atherosclerotic lesion burden as a percent of total aortic area. Group A mice, which received BM from *Pg*-infected, HFD fed donor mice, had significantly more (38%) atherosclerotic lesion compared with Group B mice, which received BM from sham-treated, HFD-fed donor mice (Figure 7B). Further analysis based on sex showed a significant 63%

increase in atherosclerotic lesion in Group A male mice compared with Group B male mice. However, female mice differed by a non-significant 16% (Figure 7C). Accordingly, we opted to do all experiments and investigations that followed on male mice only.

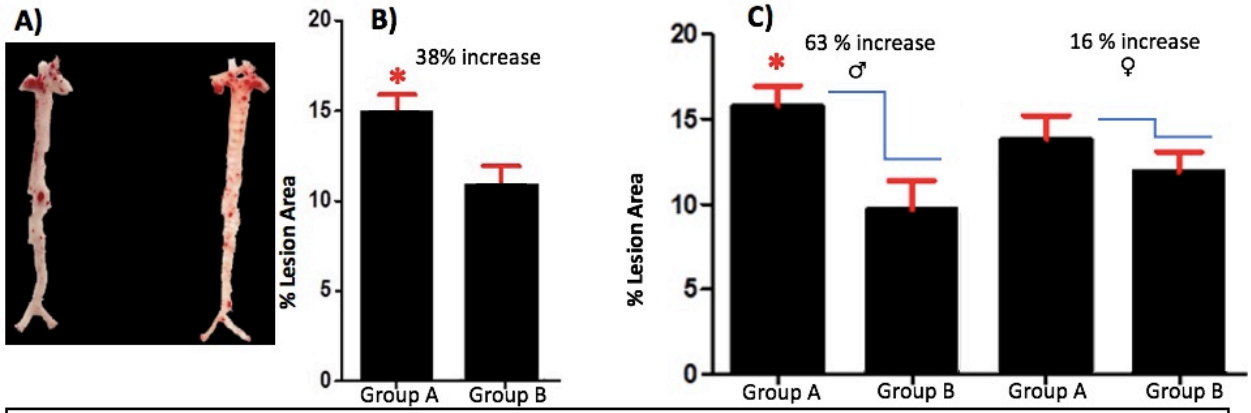

Figure 7: Group A mice developed significantly more atherosclerosis compared to Group B.

A) Representation of the mice aorta after dissection and staining with oil-red-O. The lesion burden was measured in by quantifying the lesion or red area and expressing it as percent of the entire aorta, using Adobe Photoshop software

B) Combined male and female mice that received bone marrow from *Pg*-inoculated donors (Group A, n =26) developed 38% more atherosclerosis lesion area compared with mice that received bone marrow from sham inoculated mice (Group B, n=19). * $p < 0.05$

C) Upon sex-matched data analysis, there was a significant 63% increase in atherosclerosis lesion area in male mice and a non-significant 16% increase in female mice in Group A compared to Group B. *$p < 0.01$

Group A mice have a more inflammatory blood plasma and macrophage cytokine profile compared with Group B mice

Since atherosclerosis is a chronic inflammatory disease, and *Pg* inoculation impacts gene expression contributing to atherosclerosis, then we would expect a difference in the pro-inflammatory status systemically, and in the major cell type in atherosclerosis, the macrophage. To test this hypothesis, we determined the inflammatory cytokine profile in plasma and in isolated macrophages, using The Mouse Cytokine Array Panel A.

Blood plasma was collected at time of sacrifice. In male mice that received bone marrow from *Pg*-inoculated donors (Group A), compared with male mice that received bone marrow

from sham-inoculated donors (Group B), there was a 1-4-fold increase in the pro-inflammatory cytokines Granulocyte – Colony Stimulating Factor (G-CSF), Complement 5 (C5/C5a) and Triggering Receptors Expressed on Myeloid Cells-1 (TREM-1) and a 25% decrease in expression of the anti-inflammatory cytokine, Tissue Inhibitor of Metalloprotenase-1 (TIMP-1). The anti-inflammatory cytokine, Interleukin 1 Receptor Antagonist (IL-1Ra), was also expressed at a greater level in Group A mice, but this may be in response to increased levels of IL-1, which then would be masked from measurement (Figure 8).

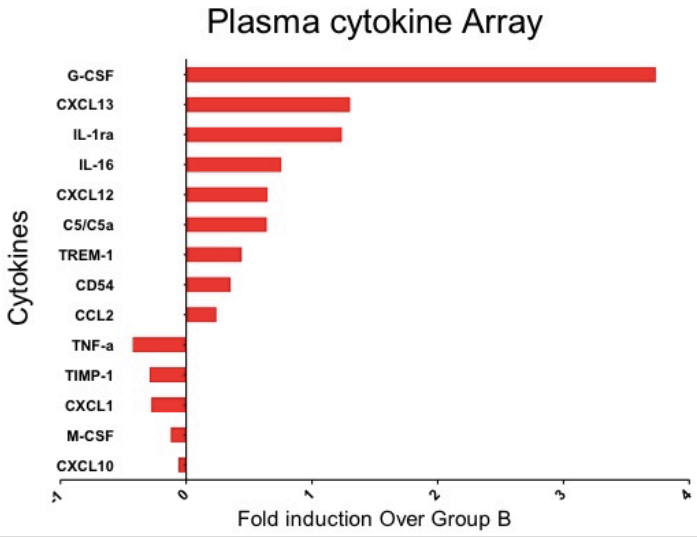

Figure 8: Group A mice have more a inflammatory plasma cytokine profile.
At time of sacrifice, 20 weeks after bone marrow transplant, blood was collected from the heart and plasma was isolated and pooled from 5 mice/group . Red bars are the expression of cytokines in recipients of bone marrow from *Pg*-inoculated donors (Group A) compared to recipients of bone marrow from sham inoculated donors (Group B). Cytokine expression was measured in duplicate. There was a 1-4-fold increase in the pro-inflammatory cytokines G-CSF, C5/C5a, and TREM-1.

Thioglycolate-elicited peritoneal macrophages were isolated at the time of sacrifice. In Group A male mice compared with Group B male mice, there was a 1-4-fold increase in the pro-inflammatory cytokines IL-7, IL-23, C-X-C Motif Chemokine Ligand 2 (CXCL2), C-C Motif Chemokine Ligand 1 (CCL1), G-CSF, CCL11, CCL12, and CXCL9 (Figure 9). Altogether, these data indicate a change in cytokine protein expression as a result of bone marrow transplant from *Pg*-infected mice. It is worth highlighting that mice were sacrificed 20 weeks after bone marrow

transplant.

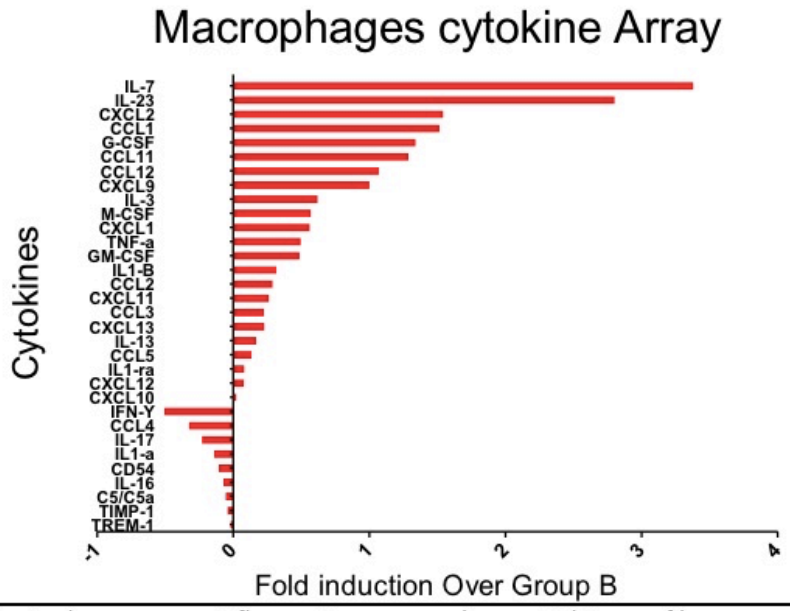

Figure 9: Group A mice have a more inflammatory macrophage cytokine profile.
At time of sacrifice, 20 weeks after bone marrow transplant, thioglycolate-elicited peritoneal macrophages were isolated and cell lysates were pooled from 5 mice/group and assessed for cytokines in duplicate. Red bars are the expression of cytokines in recipients of bone marrow from *Pg*-inoculated donors (Group A) compared to recipients of bone marrow from sham inoculated donors (Group B). Pro-inflammatory cytokines IL7, IL23, CXCL2, CCL1, G-CSF, CCL11, CCL12 and CXCL9 are expressed 1-4 fold more.

Blood cholesterol and body weight do not underlie the increase in atherosclerosis

Atherosclerosis is a multi-factorial disease; body weight and total plasma cholesterol are potential confounding factors that could impact macrophage phenotype and accentuate atherosclerosis[54,55,57]. Obesity can also impact inflammation and insulin resistance[58].

10 weeks after bone marrow transplant, blood was collected from fasted mice from the tail vein and plasma cholesterol was measured. There were no significant differences between Group A and Group B mice. At time of sacrifice, all mice were weighed, and again there were no difference between the groups (Figure 10). These data indicate that the well-established risk factors for atherosclerosis, blood cholesterol levels and body weight, do not underlie the increased atherosclerosis observed in Group A mice.

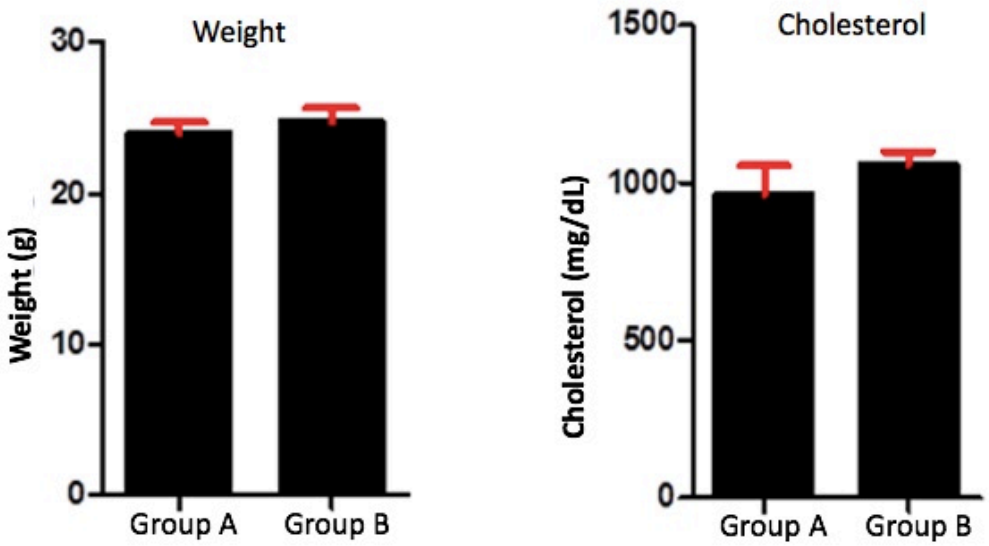

Figure 10: Neither body weight nor blood cholesterol levels underlie the increased atherosclerosis in Group A mice.
All mice were weighed at time of sacrifice and cholesterol was measured in blood plasma 10 weeks after bone marrow transplant. There were no differences between the experimental groups in body weight or blood cholesterol levels.
Group A: recipients of bone marrow from *Pg*-inoculated donors.
Group B: recipients of bone marrow from sham inoculated donors.

Whole genome bisulphite sequencing shows global hypomethylation and some hypermethylated regions in peritoneal macrophages of Group A mice

At the time of sacrifice, we isolated elicited peritoneal macrophages from both groups of recipient mice. These macrophages extravasate from the circulation in response to an inflammatory stimulus, much like in response to modified lipids in vessels[137]. Following DNA isolation and quality assurance, DNA from 5 mice/group was pooled and submitted to Novogene for whole genome bisulphite sequencing (WGBS). WGBS is considered the standard approach for genome methylation profiling[138,139]. The rationale here is to determine if DNA methylation differences underlie the observed difference in cytokine expression and atherosclerosis lesion burden. A major advantage of WGBS compared with other strategies is that it can assess the

methylation state of nearly every promoter site[138,139]. Since we cannot predict whether the difference in expression is due to methylation differences in the gene itself or a transcription factor or an upstream receptor/signalling molecule, we took a broad genome-wide approach, that should provide unbiased data.

Bisulphite conversion rate was greater than 99.6%. Mean coverage was 19.05x for mice recipients of bone marrow from *Pg*-inoculated donors (Group A), and 15.99x for mice recipients of bone marrow from sham-inoculated donors (Group B). Coverage depth was 10x for 83.48% in Group A and 73.95% for Group B. Raw base sequencing data generated 262,675,688 and 265,896,696 total reads for Group A and Group B, respectively, of which 209,297,491and 197,260,449 were uniquely mapped to the *Mus musculus* genome, resulting in unique map rates of 79.68% and 74.19% in Group A and Group B, respectively. Overall there was global hypomethylation in Group A, compared to Group B, and the cluster analysis showed hypomethylation of promoters in Group A (Figure 11). Differentially methylated promoters (DMPs) were identified with at least 0.2 methylation level difference with $p<0.05$ (Figure 12). Methylation differences at the promotor region, 2 kb upstream of the transcription start site (TSS), has potential to impact gene expression. As already mentioned, hypomethylation has been associated with increase in gene expression[108].

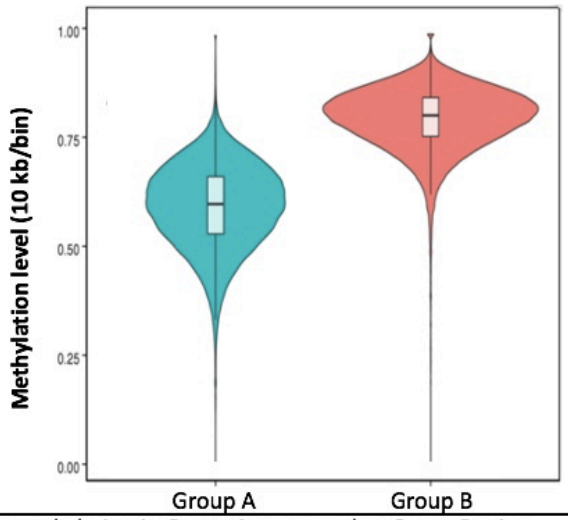

Figure 11: Global DNA hypomethylation in Group A compared to Group B mice.
WGBS of purified DNA from elicited peritoneal macrophages (5 mice/group) was done. Using 10Kb bins, the methylation level was calculated based on the ratio of methylated cytosines to total (unmethylated and methylated cytosines). The width of each violin represents the number of methylated sites in the corresponding methylation level. The rectangles in the middle of the violin represents the 25% and 75% interquartile ranges and the horizontal black line in the rectangles represents the median level of methylation.
Group A: recipients of bone marrow from *Pg*-inoculated donors.
Group B: recipients of bone marrow from sham inoculated donors.

Figure 12: More promotors are hypomethylated in Group A mice.
A) Promotor methylation assessed at a single nucleotide level 2 Kb downstream and upstream of the TSS. Comparing the blue line (group A) to the red line (group B), group A is hypomethylated throughout this 4 Kb region.
B) Hierarchical cluster analysis of each DMP presenting methylation levels from 0 (deep blue – less methylation) to 1 (deep red – more methylation), where 0 is unmethylated and 1 is completely methylated. Each line represents one DMP and columns represent the Groups. Group A has more and deeper blue whereas Group B has more and deeper red.

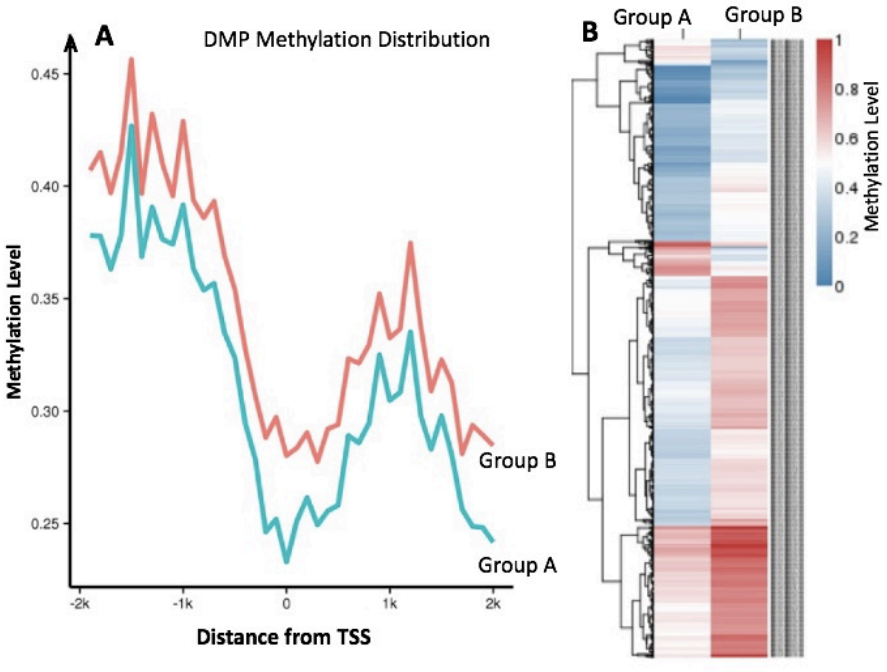

A significant correlation exists between expression of several tissue-specific genes and regions of methylated DNA. Thus, identifying differentially methylated regions (DMRs) in the DNA is critical in the functional analysis of WGBS. Given the high cost of WGBS, having

replicates is not always feasible, and in our case, we didn't have replicates but we pooled 5 samples per group, as mentioned earlier. Therefore, DMRs were identified and analyzed using the sliding window approach[140]. Through integration of various statistical methods, this approach annotates and visualizes DMRs and enables comparison between samples that do not have replicates[140]. For our data, DMRs between Groups A and B were identified using the following criteria; presence of at least 0.1 methylation level difference, more than 2-fold change, at least 10 cytosines in the specified region and $p<0.05$. Using these criteria, a total of 375 DMRs were identified, of which 217 were hypomethylated and 158 were hypermethylated in Group A compared to Group B (Figure 13). These data strongly support the hypothesis that *Pg*-mediated epigenetic changes can influence macrophage phenotype, be transferred by bone marrow transplant and perpetuate for long periods.

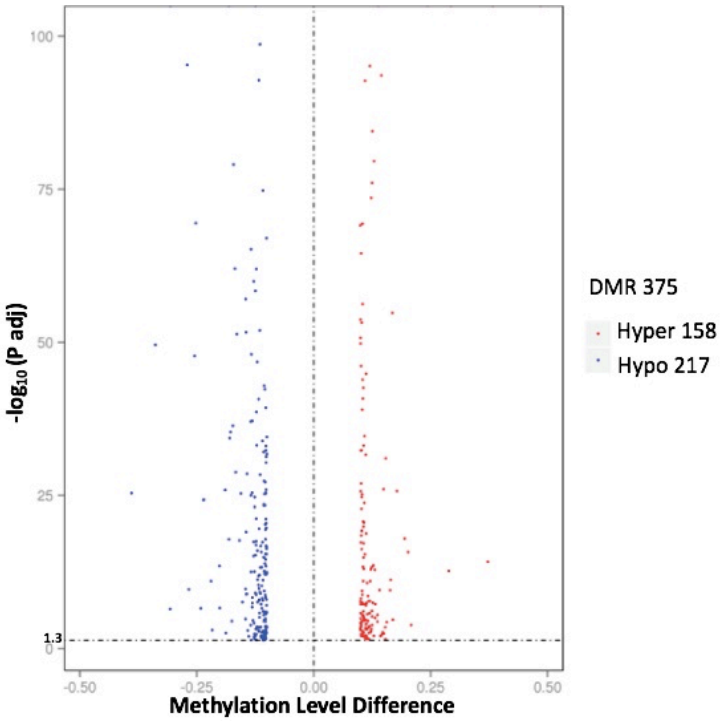

Figure 13: Volcano plot showing Group A hypomethylated(blue dots) and hypermethylated(red dots) DMRs.
Compared to Group B, Group A mice have 217 hypomethylated DMRs and 158 hypermethylated DMRs. DMRs are plotted as a function of their methylation level difference on the X-axis, and their adjusted p-value (-log 10) on the Y-axis. The cut off for significance is p adj< 0.05, which corresponds to $-\log_{10}$ value of 1.3.
Group A: recipients of bone marrow from *Pg*-inoculated donors.
Group B: recipients of bone marrow from sham inoculated donors.

Hypermethylation of the rate-limiting enzymes in the methionine cycle in Group A mice

Methionine, a sulphur-containing essential amino acid, is a critical component of the methionine cycle and the trans-sulphuration pathway (Figure 14). In the methionine cycle, the methyl group is activated by adenosine triphosphate (ATP) through the addition of adenosine to sulphur, a process catalysed by methionine adenosyl transferase (MAT). This converts methionine to SAM, the methyl universal donor[141]. Several methyltransferases, including DNMT which transfers the methyl group from SAM to carbon-5 of the cytosine ring[113,142], will then remove this methyl group, converting SAM to S-adenosylhomocysteine (SAH). Our WGBS data show a significant hypermethylation in MAT in mice recipient of bone marrow from *Pg*-inoculated donors (Group A) compared to mice recipient of bone marrow from sham-inoculated donors (Group B). Importantly, this hyper-methylation is in the 3' untranslated regions (UTR). Methylation of this specific region has been associated with degradation of MAT and in turn depletion of SAM[143]. These data suggest that hypermethylation of MAT, and the subsequent attenuation of the methionine cycle, could at least be partially responsible for the global hypomethylation observed in Group A mice.

Homocysteine, a sulphur-containing amino acid, is critically positioned at the intersection between the methionine cycle and the trans-sulphuration pathway[142] (Figure 14). SAH, a product of the SAM-dependent methylation and a potent negative feedback inhibitor of methylation, is hydrolysed to homocysteine and adenosine by SAH hydrolase (SAHH)[141,142]. Importantly, this process is reversible, where SAHH can catalyse the synthesis of SAH from homocysteine. SAHH is the only enzyme that catalyses this reversible process and hence is critical[144]. In fact, deletion of SAHH in mice is embryonic lethal[144], and deficiency of SAHH in human is associated with Wilson Disease, an incurable metabolic disorder[144].

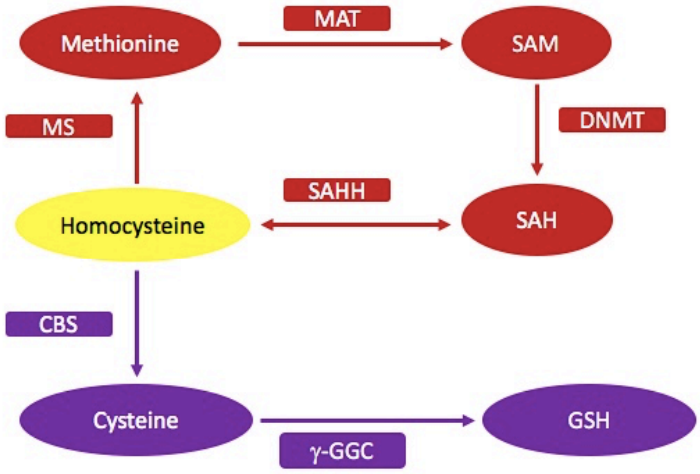

Figure 14: Simplified representation of the methionine cycle (Red) and the trans-sulphuration pathway (purple). Homocysteine is located at the intersection of the methionine cycle and the trans-sulphuration pathway. Homocysteine can revert to SAH via SAHH, remethylates to methionine via MS , or synthesizes cysteine via the trans-sulphuration pathway.
MAT: Methionine adenosyltransferase, SAM: S-adenosylmethionine , DNMT: DNA methyl transferase, SAH: S-adenosylhomocysteine, SAHH: S-adenosylhomocysteine hydrolase, CBS: Cystathionine β-synthetase , γ-GGC: γ–Glutamylycysteine, GSH: Glutathione

Our WGBS data identified a hypermethylated DMR that corresponds to GM4737, the protein coding gene for SAHH, in Group A compared to Group B mice. Remarkably, this increased methylation is located in CpG islands and CpG shores. CpG islands are defined as regions that are more than 500 bp with more than 55% cytosine-guanine, and are commonly found in promoters. CpG shore is a 2Kb region immediately flanking CpG islands. Increased methylation of both CpG islands and CpG shores have been strongly associated with decreased gene expression. Therefore, the hypermethylation of GM4737 in Group A mice strongly suggests a decreased expression of SAHH. Being the only enzyme capable of the reversible hydrolysis of SAH to homocysteine[144], this essentially suggests increase in SAH or homocysteine or both. Importantly, several studies have identified a strong and significant, and possibly synergistic, association between increased levels of homocysteine and/or increased levels of SAH and atherosclerotic CVD[145,146].

Group A mice have higher plasma SAH compared to Group B but SAM levels are not different

Given the critical opposing roles of SAM and SAH in the methionine cycle, in an attempt to validate our WGBS data of the hypermethylation of MAT and SAHH genes, we opted to measure and compare the plasma levels of SAM and SAH. At time of sacrifice, plasma was collected from mice recipient of bone marrow from *Pg*-incoulated donors (Group A) and from mice recipient of bone marrow form sham-inoculated donors (Group B), and in 3 mice/group, SAM and SAH levels were measured in duplicates via a competitive ELISA reaction. The plasma sample and primary antibody were incubated in a SAM or SAH conjugate-coated well, so that the sample and the conjugate compete to bind to the antibody. Antibodies bound to the sample were then washed away and antibodies bound to the conjugate were colorimetrically detected. The OD is directly proportional to the conjugate-bound antibodies, and hence reversibly proportional to the plasma bound antibodies. The final amount was then calculated through a standard curve. The data analysis revealed comparable plasma SAM levels in both groups (Figure 15).

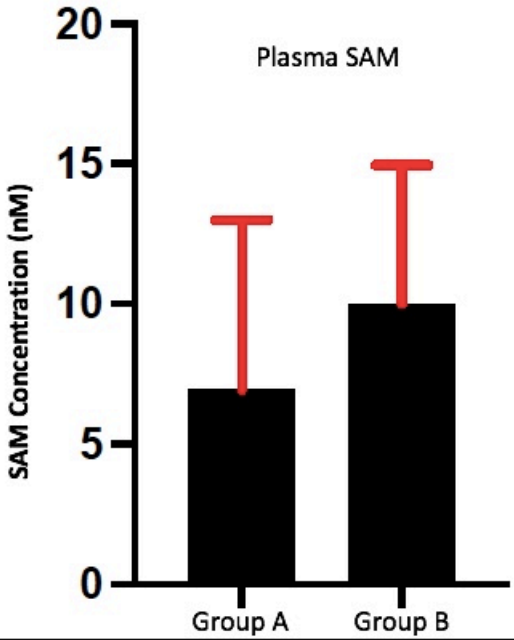

Figure 15: No significant difference in plasma SAM levels.
At time of sacrifice, plasma was collected and SAM levels were measured using an ELISA assay.
Group A: recipients of bone marrow from *Pg*-inoculated donors.
Group B: recipients of bone marrow from sham inoculated donors.

In contrast SAH levels were significantly higher in Group A mice compared to Group B, with an

increase of almost three times (Figure 16). This data is of paramount importance as it, in a way, validates the global hypomethylation, and links the hypomethylation to the increased atherosclerosis in Group A mice. It is worth mentioning that this data is from a completely separate cohort of transplanted mice, that were not fed the HFD post-transplant, to rule out diet influence. Plasma was obtained from these mice for this experiment 1year post-transplant. This suggests robust replicable epigenetic changes as a result of *Pg* infection in the context of an atherosclerotic mouse model.

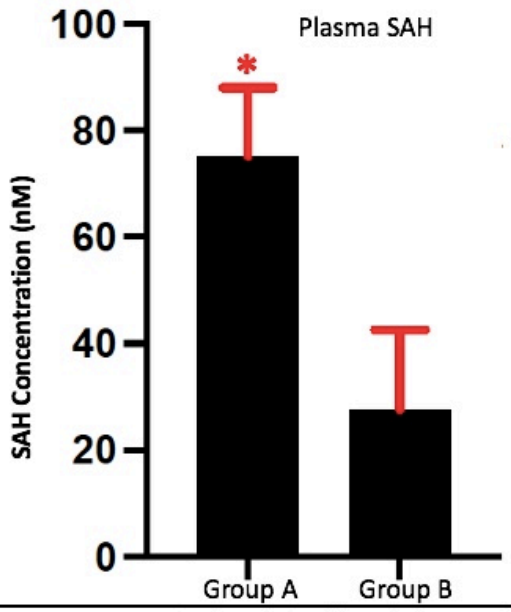

Figure 16: Group A mice have significantly more plasma SAH. At time of sacrifice, plasma was collected and SAH levels were measured using an ELISA assay. Plasma SAH levels are almost 3-fold higher in Group A mice compared to Group B mice . *p< 0.05 Group A: recipients of bone marrow from *Pg*-inoculated donors. Group B: recipients of bone marrow from sham inoculated donors.

Group A mice have significantly less DNMT activity compared to Group B

As mentioned earlier, SAH is a potent inhibitor of SAM-dependent methylation. Increased SAH has been associated with genomic global hypomethylation[144,145] and significant inhibition of SAM-dependent methyltransferases[142]. Given the global hypomethylation of mice recipient of bone marrow from *Pg*-inoculated donors (Group A) and the increase in plasma SAH levels, compared to mice recipient of bone marrow from sham-inoculated donors (Group B), we opted to compare the activity of DNMT in BMDM from Group A and Group B mice, in an attempt to identify a mechanism underlying the observed hypomethylation. For this experiment

we used the EpiQuik DNA Methyltransferase Activity/Inhibition Assay Kit by Epigentek, which measures activity in nuclear extracts. Using the EpiQuik Nuclear Extraction Kit by Epigentek, we isolated nuclear extracts from BMDM from Group A and Group B mice. This experiment was carried on 2 mice/group, that were assessed individually (not pooled) in duplicates. The nuclear extract was then incubated with a cytosine-rich DNA substrate and assay buffer containing SAM. During incubation, DNMT present in the nuclear extract transfers methyl groups from SAM to the DNA substrate. Methylated DNA was then detected by anti-5-methylcytosine antibody. The amount of methylated DNA is quantified colorimetrically through an ELISA like reaction. The amount of methylated DNA is proportional to DNMT activity. Our analysis shows that DNMT activity in Group B mice was 4X higher than that of Group A mice (Figure 17). In other words, the DNMT activity in Group A was inhibited by more than 80%. The results were consistent among different protein amounts. This data suggests that differences in DNMT activity, and not necessarily expression difference, could be the underlying mechanism of the hypomethylation observed in Group A mice.

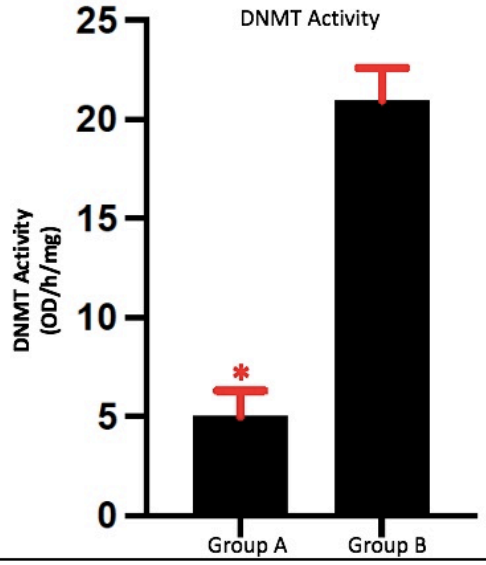

Figure 17: Group A mice have significantly less DNMT activity. Using an ELISA-like assay, we measured the activity of DNMT in BMDM nuclear extracts. DNMT activity is 4-fold higher in Group A than Group B. *p< 0.0001
Group A: recipients of bone marrow from *Pg*-inoculated donors.
Group B: recipients of bone marrow from sham inoculated donors.

Group A mice have significantly more TET activity compared to Group B

DNA methylation is governed by dual dynamic processes, namely, methylation by

DNMT enzymes, and de-methylation by TET enzymes. In the de-methylation process, the first step is the oxidation of 5mC to 5hmC[110], which is further oxidized to 5-formylcytosine (5fC) and then to 5-carboxycytosine (5caC)[147]. The latter are then excised and replaced by unmethylated cytosines in the DNA base sequence[147]. The level of methylation is hence the output of the interplay between these two opposing processes of methylation and de-methylation. Following our DNMT activity assay that suggested a rather significant inhibition in the methylation process in Group A mice, we opted to investigate the de-methylation process through analysing and comparing the TET activity in Group A and B mice. Similar to DNMT assay, we conducted this experiment on BMDM nuclear extracts, using The Epigenase™ 5mC-Hydroxylase TET Activity/Inhibition Assay Kit by Epigentik. First, we coated the microplate wells with a methylated substrate, then added the TET-containing nuclear extract to the wells. TET then oxidised 5mC to 5hmC for 90 minutes. Since 5hmC levels correlate with TET activity, a specific antibody was used to bind to the TET-converted 5hmC. The amount of 5hmC was then quantified colorimetrically by measuring the absorbance at a wavelength of 450 nm. The OD was then normalized to the amount of nuclear extract of each sample, and accordingly activity was determined. Our analysis show that TET activity was significantly higher in mice recipient of bone marrow from *Pg*-inoculated donors

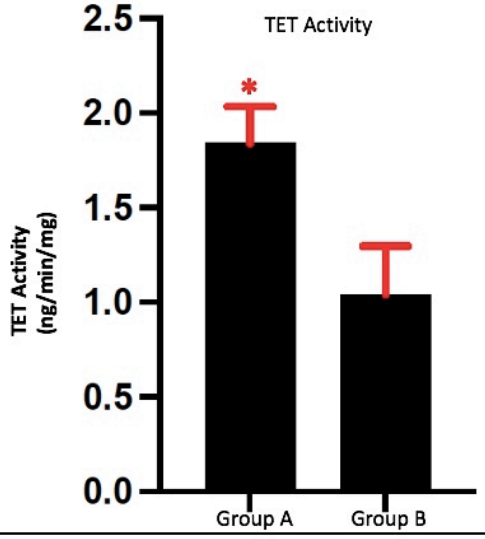

Figure 18: Group A mice have significantly more TET activity.
Using an ELISA-like assay, we measured the activity of TET in BMDM nuclear extracts. TET activity in Group A is more than 75% higher than in Group B. *p< 0.005
Group A: recipients of bone marrow from *Pg*-inoculated donors.
Group B: recipients of bone marrow from sham inoculated donors.

(Group A) compared to mice recipient of bone marrow from sham-inoculated donors (Group B). The activity in Group A was 1.7X higher than Group B mice (Figure 18). This suggests that TET-driven de-methylation is another mechanism underlying the observed hypomethylation in Group A mice. In line with that, our WGBS data shows significant hypomethylation of DMRs corresponding to TET2 gene in Group A compared to Group B mice. Importantly, the location of this decreased methylation includes CpG islands, shores and promoter regions. As mentioned earlier, methylation difference in these regions are essentially associated with gene expression. Hence, our WGBS data strongly suggest that TET2 is overexpressed in Group A mice.

CHAPTER 4

Discussion

Atherosclerosis, a chronic inflammatory disease, is the leading cause of CVD[52]. The pathophysiology of atherosclerosis is multifactorial, where the interplay between multiple risk factors increase the potential for initiation of the disease or worsening an existing condition. Atherosclerosis risk factors include age, smoking, high fat diet as well as systemic conditions such as hyperlipidemia, hypertriglyceridemia and diabetes[57-64]. Periodontal disease, a pathogen-driven chronic inflammatory disease of the periodontium, is the most common oral disease and the leading cause of tooth loss in adults[2,3,98,99]. Although the mechanisms are not clear, in the last few decades several studies have associated periodontal disease with atherosclerosis[83,84,86,87], and in 2012, the American Heart Association identified periodontal disease as an independent risk factor for atherosclerotic vascular diseases[84]. Studies are not conclusive but long term-studies suggest that treatment of periodontal disease through pathogen eradiation or even teeth extraction does not reduce subsequent risk of cardiovascular events, even after 17 years of complete edentulism[92-97,100,101]. In this project, we sought to identify the validity of this long-term sustained effect of periodontal disease, and the potential underlying mechanism of such phenomenon. DNA methylation is one of the most studied epigenetic modifications, and differences in methylation levels has been associated with periodontal disease and with atherosclerosis[114-120]. In addition, DNA methylation has been associated with sustained effects of several conditions, such as the metabolic memory phenomena observed in diabetes melitus[106,107]. In light of this information we hypothesized that periodontal disease induces changes in DNA methylation, in the self-renewing hematopoietic stem cells in the bone marrow, and these changes render macrophages more pro-atherogenic. Using the well-established atherosclerosis mouse model, the *LDLR*$^{-/-}$, we opted to simulate the circumstances of the atherosclerosis-sustained-effect of periodontal disease despite successful clinical treatment. Bone marrow cells

from atherosclerotic mice who were infected with *Pg* to induce periodontal disease, were transplanted into irradiated naïve *LDLR*$^{-/-}$ mice, who were never infected with *Pg*. Those recipient mice should therefore present the genetic and phenotypic *Pg*-induced changes in the bone marrow, but not that of elevated *Pg*.

Our model was based on a previous study completed by our lab, where we have shown that *Pg*-oral inoculation of *LDLR*$^{-/-}$ mice, significantly increased the atherosclerotic lesion burden in CD36 dependent manner[130]. This increase was associated with a pro-inflammatory systemic effect that manifested as an increase in levels of IFN-γ and IL-6[130]. In the current study, this *Pg*-induced pro-inflammatory profile was confirmed at the gene level, where we show a significant overexpression of IL1-β and IL-6 in mice orally inoculated with *Pg* compared to sham-inoculated mice. This is in accordance with several studies that have associated these cytokines with *Pg* infection and periodontal disease in mice and human[148,149]. Using bone marrow transplant in the field of atherosclerosis is not novel. In fact, it has been increasingly implemented in the field since its first use in 1995 by Linton *et al*. where they were able to prevent atherosclerosis development in the atherosclerotic mouse model, Apolipoprotein E knockout (*ApoE*$^{-/-}$), through transplanting bone marrow from wild type mice[150]. In a more recent study, Ouweneel et.al sought to determine the contribution of LDLR to the atheroprotective effect of hematopoietic ATP-binding cassette transporter A1 (*Abca1*)[151]. In this study, they transplanted bone marrow from wild-type, *LDLR*$^{-/-}$, *Abca1*$^{-/-}$, and *Abca1*$^{-/-}$ *LDLR*$^{-/-}$ to hypercholesterolemic *LDLR*$^{-/-}$. They concluded that hematopoietic Abca1 and LDLR influence development of atherosclerosis independently. The majority of the bone marrow transplant approach in the field involved chimeric mice where the recipient mouse received bone marrow cells from transgenic donors harbouring a genetic alteration in a specific pathway. However, to

the best of our knowledge, this is the first time this approach is implemented to study epigenetic changes in the association between periodontal disease and atherosclerosis.

The fundamental aim in bone marrow transplant is to reconstitute the immune system of the irradiated recipient mice with that of the donors. In our model, we hypothesized that this would manifest as an increased atherosclerotic lesion burden and a pro-inflammatory phenotype in the mice recipients of bone marrow from donors inoculated with *Pg*, consistent with the donors' manifestations shown in our previous study[130]. After 16 weeks of feeding them a HFD, Group A mice, the recipients of bone marrow from donors previously inoculated with *Pg*, developed significantly more atherosclerosis lesion burden, compared to Group B mice, who received bone marrow from sham-inoculated donors. The overall increase was 38%. Importantly, sex-based analysis revealed that the increase was more pronounced and only significant in male mice, but not in female mice.

This difference between male and female mice is in line with other studies showing sex-based differences in immune response[152]. One study showed that male mice compared to female mice produce significantly more IL-6 and LPS-binding protein upon LPS treatment, and *in vitro*, male peritoneal macrophages expressed higher level of IL-1β and TLR-4 upon LPS stimulation[153]. Mechanistically, our hypothesis implies that immune cell progenitors residing in the bone marrow from donor mice chronically inoculated with *Pg* are reprogrammed, and would give rise to more pro-inflammatory differentiated immune cells once transplanted in the recipient mice. These cells, in synergy with the pressure of HFD, or without it, would increase atherosclerotic burden.

In this study, at the systemic level, as exemplified by plasma analysis, we found increased levels of G-CSF, C5/C5a and TREM-1 and decreased TIMP-1. These cytokines have

been shown to play significant roles in atherogenesis and CVD. A recent study found a significant association between plasma G-CSF levels and major adverse cardiovascular events, including myocardial infarction and death[154]. In fact, the authors suggested using endogenous plasma G-CSF levels as an independent predictor for cardiovascular events[154]. In *ApoE*$^{-/-}$ mice, C5a was shown in multiple studies to accelerate atherogenesis and to induce disruption of atherosclerotic plaque[155,156]. This was associated with macrophage recruitment, foam cell formation and upregulation of serum TNF-α and IL-6. Furthermore, mice and human studies have identified significant association between TREM-1 and atherosclerosis. In 2018, Wang *et al.* identified a significant and independent association between plasma levels of TREM-1 and major adverse cardiovascular events as well as all-cause mortality, suggesting TREM-1 as a predictor for adverse cardiovascular events[157]. In line with that, TREM-1 was identified as a major proatherogenic receptor, that orchestrates macrophage polarization and foam cell formation through CD36 and TLR-4[158].

The sensitivity of this array for macrophages was higher than that for plasma, and our results show many more cytokines with increased expression that are associated with the atherosclerotic process. The two most differentially expressed cytokines were IL-7 and IL-23, which were expressed 4 and 3-fold more in mice recipient of bone marrow from *Pg*-inoculated donors (Group A), respectively. Both of these have been consistently associated with increased atherosclerosis in mice and human studies. In addition to being over-expressed in plasma, G-CSF was also over expressed by macrophages in Group A mice. In human, IL-7 plasma levels were significantly associated with angina, particularly the unstable form[159]. A study that used an ApoE-expressing adenovirus to regress advanced atherosclerotic lesions in *ApoE*$^{-/-}$ mice found decreased expression of IL-7, consistent with lower cholesterol, and associated with regression

of atherosclerotic lesions, and identified a role for IL-7 in recruiting monocytes and macrophages and promoting monocyte adhesion to endothelial cells[160]. Another *ApoE*$^{-/-}$ study showed that blocking the IL7-receptor after myocardial infarction, decreased macrophage and lipid content in atherosclerotic plaque[161]. Similarly, injection of anti-IL23p19 antibodies significantly reduced the expression of IL-6 and TNF-α in *ApoE*$^{-/-}$ aortas in a study that showed a significant increase of IL-23 at different time points in atherosclerotic mice compared to control mice[162]. Furthermore, a human study found that IL-23 plasma levels were significantly higher in carotid atherosclerosis patients compared to healthy controls, and the difference was more significant in symptomatic patients[163]. In the same study, the authors showed an increase in IL-23 and IL-23 receptor gene expression in carotid plaques, with colocalization in plaque macrophages[163]. Altogether, these mice and human studies indicate that, indeed, Group A mice harbour a more proatherogenic cytokine profile, and suggest that the observed increase in atherosclerosis lesion burden is driven by this profile. In line with the mentioned studies, our results are independent of other atherosclerosis risk factors, since there were no differences in blood cholesterol levels or body weight between Group A and Group B mice.

DNA methylation is the most studied epigenetic modification, and its association with specific conditions, such as cancer, revolutionized therapy and introduced an entirely new treatment approach. WGBS is considered the gold standard for a thorough and quantitative assessment of DNA methylation of the entire genome[139]. This is owed to its unbiased global approach and its ability to identify methylation level of DMPs and DMRs at single-nucleotide resolution[139]. The NIH Roadmap Epigenomics Project recommends a combined sequence depth of 30X between multiple biological replicates for whole genome analysis[138]. A recent study compared DMRs identified at different sequence depths and concluded that sequence depth of 5x

to 15x is sufficient and that higher depths are not justified[164]. They as well recommended at least 2 biological replicates. Our sequencing depth is 19.05x and 15.99x for Group A and Group B, respectively. However, given the high costs of WGBS and the fact that this was our first attempt in testing our hypothesis, we tried to compensate for not having replicates by pooling the DNA of 5 samples per group. This limitation will be addressed in our future studies by running multiple replicates of each sample. Our WGBS data indicates a global hypomethylation in mice recipient of bone marrow from *Pg*-inoculated donors (Group A) that developed more atherosclerosis lesions and harboured a more pro-atherogenic cytokine profile. This global decrease in methylation is line with major studies in the field that associated DNA global hypomethylation with increased atherosclerosis in human and animal studies. One study showed a 9% decrease in DNA methylation in advanced human atherosclerotic lesions compared to non-diseased arteries, and a 7% decrease in DNA methylation in HFD-induced atherosclerotic *ApoE*$^{-/-}$ mice compared to less-atherosclerotic chow-fed *ApoE*$^{-/-}$ mice[165]. In the same study, the authors assessed global methylation levels in rabbits after balloon denudation of the aorta, which damages the endothelium and causes proliferation of smooth muscle cells (SMC) in the intima. The proliferation of SMC was associated with a 15% decrease in DNA methylation level[165]. This level of hypomethylation was evident in normal chow and HFD rabbits, suggesting that the decreased methylation is independent of cholesterol levels in this model[165]. Importantly, these results should be interpreted cautiously, as it is not clear if the decreased methylation contributes to the SMC proliferation or a consequence of SMC proliferation. A more recent study reported a 2.5-fold decrease in global DNA methylation in human atherosclerotic arteries compared to healthy arteries, and this was associated with increased gene expression[166]. Furthermore, a 2015 human study associated hypomethylation of long interspersed nuclear element-1 (LINE-1) with

increased risk of myocardial infarction[167]. Since LINE-1 approximately compromises 17% of the human genome[168], the extent of its methylation is considered a surrogate marker of global DNA methylation. The aforementioned studies suggest that global DNA hypomethylation is a characteristic of atherosclerosis, however, this is not conclusive. In fact, there are several studies that suggest global hypermethylation as a characteristic of atherosclerosis. Yamada *et al*. identified 2272 hypermethylated CpG sites in Japanese atherosclerotic plaque compared to 407 hypomethylated sites[169]. Using WGBS, Zaina *et al*. reported to have identified a unique atherosclerosis signature, characterized by global DNA hypermethylation in human atherosclerotic vessels[170].

The pattern of global DNA hypomethylation observed in our study and other atherosclerosis studies is similar to what has been observed in other diseases, including cancer, as well as non-tumor conditions, such as diabetes and systemic lupus erythematosus[171]. The apparent discrepancy between global DNA hypomethylation and hypermethylation being a characteristic of atherosclerosis could represent population-based differences or could be due to an inherent biological issue. One issue is the fact that longer stretches of DNA are demethylated and therefore reaching a statistically significant change at any particular CpG is less frequent than reaching a statistically significant change in the relatively rare sites of hypermethylation, and, accordingly, concluding that hypermethylation predominates in atherosclerosis. Nevertheless, these controversial studies point to the infancy of our understanding of the topic and warrant further studies on the association between DNA methylation and atherosclerotic CVD.

Our WBGS data identified 217 hypomethylated and 158 hypermethylated DMRs, as well as hypomethylation of promotors close to the TSS. This localization strongly suggests an impact

on gene expression[172]. The analysis and validation of each of these differentially methylated DMRs is warranted but goes beyond the scope of this dissertation. Interestingly, we noticed that some of the identified DMRs are associated with active methylation or active de-methylation. MAT, the enzyme responsible for catalyzing the conversion of methionine to the universal methyl-donor, SAM, was hypermethylated in Group A mice, which suggests decreased expression. GM4737, the protein coding gene for SAHH, was also hypermethylated. SAHH catalyses hydrolysis of SAH, a potent methylation inhibitor, to homocysteine and adenosine. This is a reversible reaction, and interestingly, SAHH under-expression has been associated with overexpression of both SAH and homocysteine[144-146]. In contrast, TET2, one of the de-methylation enzymes, and Sirt1, an enzyme that modulates activity of DNMT1, were hypomethylated. Altogether, considering all these "methylation-determining" enzymes being differentially methylated, we sought to investigate the potential mechanism underlying the observed global hypomethylation in Group A mice and its association to the increased atherosclerosis observed.

DNMT1, the maintenance methyl transferase enzyme, has been repeatedly reported to be under-expressed and inhibited in cases of global hypomethylation, and has been associated with increased atherogenesis[165,173,174]. Our activity assay determined that DNMT is 4 times more active in mice recipient of bone marrow from sham-inoculated donors (Group B) compared to mice recipient of bone marrow from *Pg*-inoculated donors (Group A). This is in line with a study that investigated the effect of hyperlipidaemia and hyperhomocysteinemia on atherogenesis in *ApoE*$^{-/-}$ mice[175]. In this study, the hyperlipidaemia/hyperhomocysteinemia-induced increase in atherosclerosis was associated with global DNA hypomethylation, decreased DNMT1 gene expression and activity[175]. Similar results were reported in a human study that assessed the

activity of DNMT in atherosclerosis patients with hyperhomocyteinemia[176]. In this study, decreased expression and activity of DNMT was associated with increased expression of Platelet Derived Growth Factor (PDGF) in endothelial cells, which enhanced the proliferation and migration of vascular smooth muscle cells. It is worth mentioning that these 2 studies assessed DNMT activity utilizing the same kit we used. Echoing the controversy mentioned earlier between global DNA hypomethylation or hypermethylation, an *in vitro* study using THP-1 macrophages showed that human VLDL/LDL lipoprotein mix induced global DNA hypermethylation and importantly, this was associated with increased expression of DNMT1[177]. In essence, despite the discrepancy, studies seem to agree that DNMT1 plays a critical role is determining methylation levels in atherosclerosis.

In addition to the passive de-methylation that results from decrease in or loss of DNMT activity, active DNA de-methylation is caried out by TET enzymes[110]. Upon assessment of TET activity in BMDM, our data indicate that TET activity in Group A mice is almost double that in Group B mice. In addition, our WGBS data indicate that the promotor region of TET2 is hypomethylated in Group A mice, which is suggestive of overexpression. The first step of TET-induced de-methylation is the hydrolysis of 5mC to 5hmC[110]. Our findings are in contrast to a recent study that compared global levels of 5hmC in cell-free DNA in coronary artery disease (CAD) patients to normal coronary artery subjects. In this study, the authors reported significantly higher 5hmC enrichment in CAD patients, which is suggestive of higher TET activity[178]. They further reported an association between 5hmC levels and incidence of acute myocardial infarction in CAD patients, suggesting using 5hmC as a diagnostic marker for CAD and a predictor of acute myocardial infarction[178]. However, it is important to emphasize that the global assessment of 5hmC levels or TET activity may not be necessarily reflective of

intralesional functional expression. In fact, intralesional expression of TET has been shown to be athero-protective in several studies. In 2016, a study done on *ApoE*$^{-/-}$ mice showed that TET2 expression in atherosclerotic plaque was associated with decreased expression of ICAM-1, VCAM-1, and IL1-β, and this was associated with significantly less atherosclerosis[179].

Homocysteine, a non-protein forming amino acid, is strategically located at the intersection of the methionine cycle and the trans-sulphuration pathway (Figure 14). In fact, the only source of homocysteine is through the methionine cycle, where in the presence of MAT, methionine is converted to SAM, which is in turn demethylated to SAH by various methyltransferases[141,142]. In a reversible reaction, SAH is hydrolysed to homocysteine. At this point, homocysteine has three options (Figure 14). 1) it converts back to SAH via SAHH, 2) it remethylates to methionine through methionine synthase (MS), 3) it is synthesized to cysteine through the trans-sulphuration pathway in the presence of the rate limiting enzyme, cystathionine β-synthetase (CBS). The fate of homocysteine is governed by several factors, including diet, medications, pathological conditions, as well as tissue-specific differences.

Glutathione (GSH), the end-product of the trans-sulphuration pathway, is one of the fundamental antioxidants synthesized in cells[180]. Hence, under conditions of oxidative stress, synthesis of cysteine and eventually GSH through the trans-sulphuration pathway is favored over remethylating homocysteine to methionine. Therefore, conditions of oxidative stress could result in hypomethylation. Importantly, due to lack of CBS and/or cystathionase, the last enzyme in the complete trans-sulphuration pathway, not all cells are capable of shifting to the trans-sulphuration pathway and synthesizing cysteine and glutathione[181,182]. Indeed, the complete trans-sulphuration pathway was shown only in the pancreas, kidney, liver and small intestine[181,182]. Hence, in cells not capable of that, oxidative stress could lead to accumulation of

homocysteine. Under such conditions, homocysteine could be pressured to convert to SAH, which as mentioned earlier, is a potent methylation inhibitor. Indeed, the majority of mammalian cells do not express CBS[181], and hence are particularly vulnerable to homocysteine/SAH accumulation. Using the same study design, our lab assessed DNA methylation in bone marrow progenitor cells using WGBS, and performed a transcriptome analysis in BMDM using RNAseq. Group A mice displayed methylation and expression changes consistent with a pro-oxidative phenotype. Based on those data and this study's macrophage WGBS data that showed hypermethylation of the rate limiting enzymes, MAT and SAHH, we opted to analyze plasma levels of SAM and SAH. SAH plasma levels were significantly higher in mice recipient of bone marrow from *Pg*-inoculated donors (Group A) compared to mice recipient of bone marrow from sham-inoculated donors (Group B).

This result is rather expository for multiple reasons. Firstly, it validates and strongly suggests a mechanism for our global hypomethylation data revealed by the WGBS. Actually, increased levels of SAH were shown to directly inhibit DNMT1 activity by up to 70%, and other SAM-dependent methyl transferases by up to 90%[142]. In contrast, experimentally inhibiting SAHH with adenosine-2,3-dialdehyde in endothelial cells, resulted in increased intracellular SAH and decreased DNA methylation[183]. Secondly, it suggests a mechanistic link between global hypomethylation and increased atherosclerosis in Group A mice. Several studies have associated plasma SAH levels with CVD and atherosclerosis[184]. In a case-controlled study, plasma SAH levels were significantly higher in CVD patients compared to healthy controls, leading the authors to suggest using plasma SAH levels as sensitive indicator for CVD risk[185]. A more recent prospective cohort study on 1003 patients undergoing coronary angiography reported a significant association between plasma SAH levels and increased risk of stroke and

non-fatal myocardial infarction[186]. Experimentally, in a series of studies, Luo *et al*. and Xiao *et al*. inhibited SAHH in *ApoE*$^{-/-}$ mice by feeding them an adenosine-2,3-dialdehyde-supplemented diet[187,188]. After 8, 16 weeks and 24 weeks, there were significant increases in plasma SAH levels associated with accelerated development of atherosclerotic lesions[187,188].

Mechanistically, other than its role in passive DNA de-methylation, the role of SAH in increasing atherosclerosis is not fully understood. Several studies proposed induction of oxidative stress as a potential mechanism. An *in vitro* study reported that intracellular accumulation of SAH in endothelial cells resulted in significantly higher expression of nicotinamide adenine dinucleotide phosphate oxidase (NOX) and the production of ROS[189]. This was associated with apoptosis[189]. In contrast, increased plasma SAH levels in *ApoE*$^{-/-}$ mice via methionine-supplemented diet or through inhibition of SAHH, induced proliferation and migration of vascular smooth muscle cells via an oxidative stress-dependent activation of the extracellular signal-regulated protein kinase (ERK) pathway[187]. In addition, our results show lower plasma SAM levels in mice recipient of bone marrow from *Pg*-inoculated donors (Group A) compared to mice recipient of bone marrow from sham-inoculated donors (Group B). Although the difference is not statistically significant, in combination with the increased levels of SAH, the resultant SAM:SAH ratio is lower in Group A compared to Group B. The ratio between SAM and SAH has been referred to as the methylation index or methionine index and has been repeatedly positively corelated with global DNA methylation levels. Hence, the lower SAM:SAH ratio in Group A mice is in line, and possibly underlies the global DNA hypomethylation. Importantly, this ratio has been associated with atherosclerosis and CVD. In contrast with our findings, an *ApoE*$^{-/-}$ mice study reported a significant association between increased plaque size and plasma SAH elevated levels as well as SAM:SAH ratio[190]. Another

study that compared healthy controls to peripheral arterial occlusive disease patients, reported increased SAH and decreased SAM:SAH ratio in patients, both in plasma and in erythrocytes[191].

Based on our results in this dissertation, we propose that *Pg*-induced periodontal disease in the atherosclerotic mouse model , *LDLR*$^{-/-}$, possibly through oxidative stress, which has been shown to increase in periodontal disease patients [192-194], creates an epigenetic pressure in bone marrow cells. This epigenetic pressure manifests as global DNA hypomethylation, and is associated with increased atherosclerosis. One potential mechanism is through SAH-driven disruption of the methionine cycle. Whether oxidative stress, either *Pg*-induced or as a result of increased SAH, underlies the initiation and sustainability of this disruption, as well as the role of SAHH is yet to be examined (Figure 19).

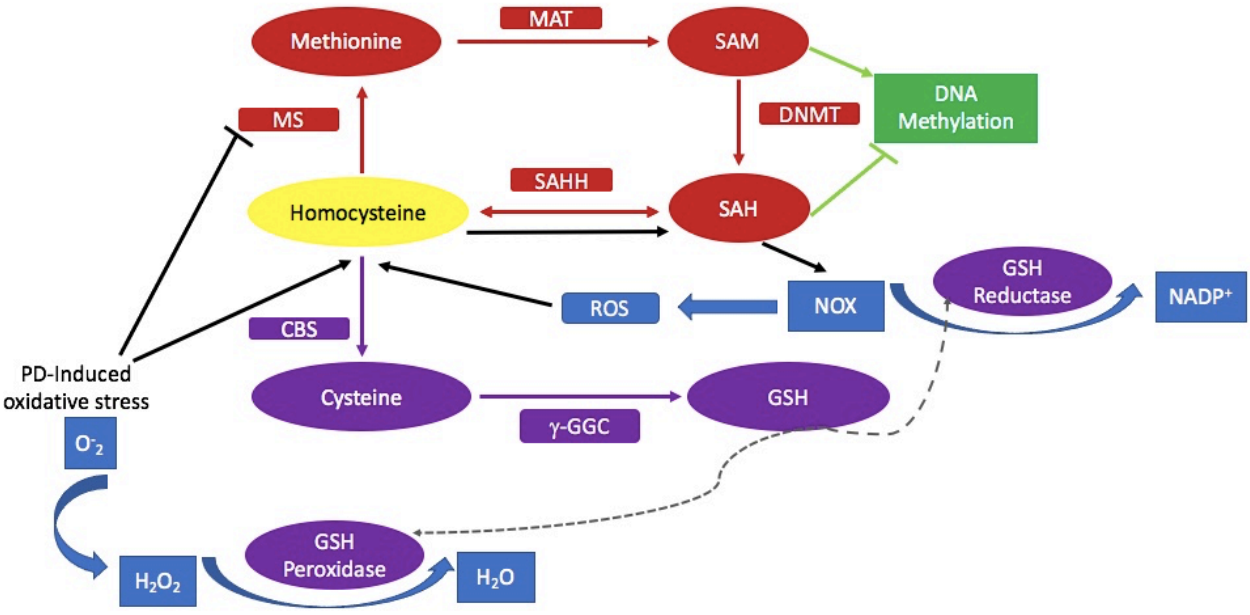

Figure 19: We propose that periodontal disease-induced oxidative stress, decreases the activity of MS and hence, less Homocysteine is remethylated to methionine. In turn, more Homocysteine will be hydrolyzed to SAH through SAHH. The oxidative stress as well pushes Homocysteine to synthesize cysteine and subsequently the antioxidant GSH. NOX and formation of ROS as a result of increased SAH, could have similar effects. Altogether, this leads to DNA hypomethylation. PD: Periodontal disease, MAT: Methionine adenosyltransferase, SAM: S-adenosylmethionine , DNMT: DNA methyl transferase, SAH: S-adenosylhomocysteine, SAHH: S-adenosylhomocysteine hydrolase, CBS: cystathionine β-synthetase , γ-GGC: γ– Glutamylycysteine, GSH: Glutathione, NOX: Nicotinamide adenine dinucleotide phosphate oxidase, ROS: Reactive Oxygen Species.

It is important to emphasize a critical limitation in our study. As mentioned earlier, the aetiology of periodontal disease is periodontal pathogen in a susceptible host. In our model, we used *Pg* as periodontal pathogen to induce periodontal disease, however, we do not replicate the critical host susceptibility factor. Therefore, our results and observations in this study do not allow us to draw conclusions regarding the sustained increased risk of atherosclerosis in treated periodontal disease patients. However, what we are proposing is paradigm shifting and warrants further studies to explore the need and necessity to modify treatment of periodontal disease.

Another potential limitation of this study is that we did not test for possible *Pg*-induced changes in the gut microbiota. Emerging evidence has shown that *Pg* oral inoculation in mice results in changes in composition of the gut microbiota which was associated with altering the serum metabolite profile[195]. Importantly, some of these metabolite alterations, such as changes in branched-chain amino acids and aromatic amino acids have been associated with CVD and diabetes[196]. Addressing this limitation would not contradict or undermine what we are proposing, but could rather enhance our understanding and interpretation of the results presented in this project.

It is as well noteworthy that most mice, including $LDLR^{-/-}$, do not get myocardial infarction despite developing atherosclerosis, this inherent limitation could explain some discrepancies between mice studies and patients.

This is an ongoing project in our lab with a lot of potential to identify more mechanisms and specific genes and pathways associated with the observed phenotype of increased atherosclerosis. We will continue to analyse our differentially methylated DMRs using gene ontology (http://www.geneontology.org/), and identify their different roles in biological systems through KEGG (http://www.kegg.jp/). Based on the results presented in this dissertation, future

experiments will attempt to further validate the results and test the validity of our proposal. One of the proposals we are making is that periodontitis-induced oxidative stress underlies the DNA methylation changes in hematopoietic stem cells of *Pg*-inoculated donors, and the increased atherosclerosis lesion burden in mice recipients of bone marrow from *Pg*-inoculated donors. This proposition could be validated by assessing and comparing oxidative stress in recipient mice. This can be done directly through measuring levels of ROS or indirectly through measuring levels of markers of DNA/RNA damage, such as 8-hydroxydeoxyguanosine, and/or measuring levels of lipid peroxidation markers such as malondialdehyde. Further, in an attempt to revert or decrease the periodontitis-induced methylation changes, we can treat *Pg*-inoculated donors with anti-oxidants, and determine if this attenuated the increased atherosclerosis in recipients of bone marrow from *Pg*-inoculated donors.

In this dissertation, we explored in depth one mechanism for DNA methylation, namely the methionine cycle. Our results suggest a role for TET2 which warrants further exploration, as it could represent another important mechanism underlying the observed DNA hypomethylation. To the best of our knowledge, this is the first study that explores the role of epigenetics in the sustained association between treated periodontal disease and atherosclerosis. Our promising results should encourage investigating other epigenetics mechanisms, such as histone modifications.

Designing medications targeting epigenetic activity has gained traction in recent years, and is one of the promising fields in medicine and pharmacology. In fact, significant success has been achieved in the field of cancer, where histone deacetylation inhibitors and DNMT inhibitors have been approved for treatment of different malignancies by the Food and Drug Administration and the European Medicines Agency[197]. Identifying and therapeutically targeting

epigenetic process in atherosclerosis and its risk factors could represent a milestone in our long fight against the leading cause of mortality, CVD.

References:

1) Lindhe J, Lang N P, Berglundh T, Giannobile W V, Sanz M. Clinical Periodontology and Implant Dentistry. 7th edition. Oxford: Blackwell Munksgaard; 2021 (pp.3-34).
2) Könönen E, Gursoy M, Gursoy UK. Periodontitis: A Multifaceted Disease of ToothSupporting Tissues. Journal of Clinical Medicine 2019 8(8):1135.
3) Khan SA, Kong EF, Meiller TF, Jabra-Rizk M. Periodontal Diseases: Bug Induced, Host Promoted. PLoS Pathogens 2015 11(7):e1004952.
4) Hajishengallis G, Lamont RJ. Beyond the red complex and into more complexity: The polymicrobial synergy and dysbiosis (PSD) model of periodontal disease etiology. Molecular Oral Microbiology 2012 27(6):409-419.
5) Kilian M, Chapple IL, Hannig M, Marsh PD, Meuric V, Pedersen AM, Tonetti MS, Wade WG, Zaura E. The oral microbiome - an update for oral healthcare professionals. Br Dent J. 2016 221(10):657-666.
6) Colombo APV, Boches SK, Cotton SL, Goodson JM, Kent R, Haffajee AD, et al. Comparisons of Subgingival Microbial Profiles of Refractory Periodontitis, Severe Periodontitis, and Periodontal Health Using the Human Oral Microbe Identification Microarray. J Periodontol 2009 80(9):1421-1432.
7) Suzuki N, Yoneda M, Hirofuji T. Mixed Red-Complex Bacterial Infection in Periodontitis. International Journal of Dentistry 2013 2013:587279.
8) How KY, Song KP and Chan KG. Porphyromonas gingivalis: An Overview of Periodontopathic Pathogen below the Gum Line. Frontiers in microbiology. 2016 7:53.
9) Loesche W. J. Chemotherapy of dental plaque infections. Oral Sci. Rev.1976 9, 65–107.
10) Hajishengallis G, Darveau RP and Curtis MA. The keystone-pathogen hypothesis. Nature reviews Microbiology. 2012 10:717-25.
11) Darveau RP, Hajishengallis G and Curtis MA. Porphyromonas gingivalis as a potential community activist for disease. Journal of dental research. 2012 91:816-20.
12) Chen T, Nakayama K, Belliveau L, Duncan MJ. *Porphyromonas gingivalis* gingipains and adhesion to epithelial cells. Infect Immun 2001 69(5):3048-3056.
13) Löe H, Anerud A, Boysen H, Morrison E. Natural history of periodontal disease in man. Rapid, moderate and no loss of attachment in Sri Lankan laborers 14 to 46 years of age. J Clin Periodontol. 1986 13(5):431-45.
14) Löe H, Anerud A, Boysen H, Smith M. The natural history of periodontal disease in man. The rate of periodontal destruction before 40 years of age. J Periodontol. 1978 49(12):607-20.
15) Löe H, Anerud A, Boysen H. The natural history of periodontal disease in man: prevalence, severity, and extent of gingival recession. J Periodontol. 1992 63(6):489-95.
16) Kornman, K.S. and di Giovine, F.S. Genetic Variations in Cytokine Expression: A Risk Factor for Severity of Adult Periodontitis. Annals of Periodontology,1998 3:327-338.

17) Umesh S.G, Ramachandran L, Karthikeyan J, Mani A, Periodontology - Fundamentals and Clinical Features. 1st edition. Intechopen; 2021.
18) Chapple IL, Genco R; working group 2 of the joint EFP/AAP workshop. Diabetes and periodontal diseases: consensus report of the Joint EFP/AAP Workshop on Periodontitis and Systemic Diseases. J Periodontol. 2013 84(4 Suppl):S106-12.
19) Taylor JJ, Preshaw PM, Lalla E. A review of the evidence for pathogenic mechanisms that may link periodontitis and diabetes. J Clin Periodontol. 2013 40 Suppl 14:S113-34.
20) Löe H. Periodontal disease. The sixth complication of diabetes mellitus. Diabetes Care. 1993 16(1):329-34.
21) Bergström J, Eliasson S, Dock J. A 10-year prospective study of tobacco smoking and periodontal health. J Periodontol. 200071(8):1338-47.
22) Bergström J, Eliasson S. Noxious effect of cigarette smoking on periodontal health. J Periodontal Res. 1987 22(6):513-7.
23) Bergström J, Eliasson S, Dock J. Exposure to tobacco smoking and periodontal health. J Clin Periodontol. 2000 27(1):61-8.
24) Armitage GC. Development of a classification system for periodontal diseases and conditions. Ann Periodontol. 1999 4(1):1-6.
25) . The American Academy of Periodontology. Proceedings of the World Workshop in Clinical Periodontics. Chicago, IL: American Academy of Periodontology; 1989:1-22
26) Caton JG, Armitage G, Berglundh T, Chapple ILC, Jepsen S, Kornman KS, Mealey BL, Papapanou PN, Sanz M, Tonetti MS. A new classification scheme for periodontal and peri-implant diseases and conditions - Introduction and key changes from the 1999 classification. J Clin Periodontol. 2018 45 Suppl 20:S1-S8.
27) Lang NP, Bartold PM. Periodontal health. J Periodontol. 2018 89 Suppl 1:S9-S16.
28) Murakami S, Mealey BL, Mariotti A, Chapple ILC. Dental plaque-induced gingival conditions. J Periodontol. 2018 89 Suppl 1:S17-S27.
29) Holmstrup P, Plemons J, Meyle J. Non-plaque-induced gingival diseases. J Periodontol. 2018 Jun;89 Suppl 1:S28-S45.
30) Trombelli L, Farina R, Silva CO, Tatakis DN. Plaque-induced gingivitis: Case definition and diagnostic considerations. J Clin Periodontol. 2018 45 Suppl 20:S44-S67.
31) Chapple ILC, Mealey BL, Van Dyke TE, Bartold PM, Dommisch H, Eickholz P, Geisinger ML, Genco RJ, Glogauer M, Goldstein M, Griffin TJ, Holmstrup P, Johnson GK, Kapila Y, Lang NP, Meyle J, Murakami S, Plemons J, Romito GA, Shapira L, Tatakis DN, Teughels W, Trombelli L, Walter C, Wimmer G, Xenoudi P, Yoshie H. Periodontal health and gingival diseases and conditions on an intact and a reduced periodontium: Consensus report of workgroup 1 of the 2017 World Workshop on the Classification of Periodontal and Peri-Implant Diseases and Conditions. J Periodontol. 2018 89 Suppl 1:S74-S84.
32) Fine DH, Patil AG, Loos BG. Classification and diagnosis of aggressive periodontitis. J Periodontol. 2018 89 Suppl 1:S103-S119.
33) Needleman I, Garcia R, Gkranias N, Kirkwood KL, Kocher T, Iorio AD, Moreno F, Petrie A. Mean annual attachment, bone level, and tooth loss: A systematic review. J Periodontol. 2018 89 Suppl 1:S120-S139.
34) Tonetti MS, Greenwell H, Kornman KS. Staging and grading of periodontitis: Framework and proposal of a new classification and case definition. J Periodontol. 2018 89 Suppl 1:S159-S172..

35) Papapanou PN, Sanz M, Buduneli N, Dietrich T, Feres M, Fine DH, Flemmig TF, Garcia R, Giannobile WV, Graziani F, Greenwell H, Herrera D, Kao RT, Kebschull M, Kinane DF, Kirkwood KL, Kocher T, Kornman KS, Kumar PS, Loos BG, Machtei E, Meng H, Mombelli A, Needleman I, Offenbacher S, Seymour GJ, Teles R, Tonetti MS. Periodontitis: Consensus report of workgroup 2 of the 2017 World Workshop on the Classification of Periodontal and Peri-Implant Diseases and Conditions. J Periodontol. 2018 89 Suppl 1:S173-S182.
36) Albandar JM, Susin C, Hughes FJ. Manifestations of systemic diseases and conditions that affect the periodontal attachment apparatus: Case definitions and diagnostic considerations. J Periodontol. 2018 89 Suppl 1:S183-S203.
37) Jepsen S, Caton JG, Albandar JM, Bissada NF, Bouchard P, Cortellini P, Demirel K, de Sanctis M, Ercoli C, Fan J, Geurs NC, Hughes FJ, Jin L, Kantarci A, Lalla E, Madianos PN, Matthews D, McGuire MK, Mills MP, Preshaw PM, Reynolds MA, Sculean A, Susin C, West NX, Yamazaki K. Periodontal manifestations of systemic diseases and developmental and acquired conditions: Consensus report of workgroup 3 of the 2017 World Workshop on the Classification of Periodontal and Peri-Implant Diseases and Conditions. J Periodontol. 2018 89 Suppl 1:S237-S248.
38) Loesche WJ. The antimicrobial treatment of periodontal disease: changing the treatment paradigm. Crit Rev Oral Biol Med. 1999 10(3):245-75.
39) Badersten A, Nilveus R, Egelberg J. Effect of nonsurgical periodontal therapy. II. Severely advanced periodontitis. J Clin Periodontol. 1984 11(1):63-76.
40) Badersten A, Nilvéus R, Egelberg J. Effect of nonsurgical periodontal therapy. I. Moderately advanced periodontitis. J Clin Periodontol. 19818(1):57-72.
41) Greenstein G. Nonsurgical periodontal therapy in 2000: a literature review. J Am Dent Assoc. 2000 131(11):1580-92.
42) Löe H. Mechanical and chemical control of dental plaque. J Clin Periodontol. 1979 6(7):32-6.
43) Hirschfeld L, Wasserman B. A long-term survey of tooth loss in 600 treated periodontal patients. J Periodontol. 1978 49(5):225-37.
44) McFall WT Jr. Tooth loss in 100 treated patients with periodontal disease. A long-term study. J Periodontol. 1982 53(9):539-49
45) Lindhe J, Nyman S. Long-term maintenance of patients treated for advanced periodontal disease. J Clin Periodontol. 1984 11(8):504-14.
46) Wilson TG Jr, Glover ME, Schoen J, Baus C, Jacobs T. Compliance with maintenance therapy in a private periodontal practice. J Periodontol. 1984 55(8):468-73.
47) Page RC, Schroeder HE. Pathogenesis of inflammatory periodontal disease. A summary of current work. Lab Invest. 1976 (3):235-49.
48) Lindhe J, Lang N P, Berglundh T, Giannobile W V, Sanz M. Clinical Periodontology and Implant Dentistry. 7th edition. Oxford: Blackwell Munksgaard; 2021 (pp.241-256)
49) Hasturk H, Kantarci A, Van Dyke TE. Oral inflammatory diseases and systemic inflammation: role of the macrophage. Front Immunol. 2012 May 16; 3:118.
50) Miller CS, King CP, Jr., Langub MC, Kryscio RJ and Thomas MV. Salivary biomarkers of existing periodontal disease: a cross-sectional study. J Am Dent Assoc. 2006 137:322-9.

51) Graves DT, Fine D, Teng YT, Van Dyke TE, Hajishengallis G. The use of rodent models to investigate host-bacteria interactions related to periodontal diseases. J Clin Periodontol. 2008 Feb 35(2):89-105
52) Roth GA, Abate D, Abate KH, Abay SM, Abbafati C, Abbasi N, et al. Global, regional, and national age-sex-specific mortality for 282 causes of death in 195 countries and territories, 1980–2017: A systematic analysis for the global burden of disease study 2017. The Lancet 2018 392(10159):1736-1788.
53) Virani SS, Alonso A, Aparicio HJ, Benjamin EJ, Bittencourt MS, Callaway CW, Carson AP, Chamberlain AM, Cheng S, Delling FN, Elkind MSV, Evenson KR, Ferguson JF, Gupta DK, Khan SS, Kissela BM, Knutson KL, Lee CD, Lewis TT, Liu J, Loop MS, Lutsey PL, Ma J, Mackey J, Martin SS, Matchar DB, Mussolino ME, Navaneethan SD, Perak AM, Roth GA, Samad Z, Satou GM, Schroeder EB, Shah SH, Shay CM, Stokes A, VanWagner LB, Wang NY, Tsao CW; American Heart Association Council on Epidemiology and Prevention Statistics Committee and Stroke Statistics Subcommittee. Heart Disease and Stroke Statistics-2021 Update: A Report From the American Heart Association. Circulation. 2021 143(8):e254-e743
54) Statistics Canada. Table 13-10-0394-01 Leading causes of death, total population, by age group. Available from: https://www150.statcan.gc.ca/t1/tbl1/en/tv.actiºn?pid=1310039401
55) Statistics Canada. Causes of Death, Canada 2011. CANSIM data. 2014. Avaliable from:

https://www150.statcan.gc.ca/n1/pub/82-625-x/2014001/article/11896-eng.htm

56) The Public Health Agency in Canada. The Economic Burden of Illness in Canada, 2010. 2017; Available from: https://www.canada.ca/en/public-health/services/publications/science-research-data/economic-burden-illness-canada-2010.html#cost. [cited June 20, 2020].
57) Mahmood SS, Levy D, Vasan RS, Wang TJ. The Framingham Heart Study and the Epidemiology of Cardiovascular Disease: A Historical Perspective. The Lancet 2014 383(9921):999-1008.
58) Framingham Heart Study: Three Generations of Dedication. Epidemiological Background and Design: The Framingham Heart Study. Available from: https://framinghamheartstudy.org/fhs-about/history/epidemiological-background/. [cited May 1, 2020].
59) Castelli WP, Garrison RJ, Wilson PWF, Abbott RD, Kalousdian S, Kannel WB. Incidence of Coronary Heart Disease and Lipoprotein Cholesterol Levels: The Framingham Study. JAMA 1986 256(20):2835-2838.
60) Stamler J, Wentworth D, Neaton JD. Is Relationship Between Serum Cholesterol and Risk of Premature Death From Coronary Heart Disease Continuous and Graded?: Findings in 356 222 Primary Screenees of the Multiple Risk Factor Intervention Trial (MRFIT). JAMA 1986 256(20):2823-2828.
61) Castelli WP. The triglyceride issue: A view from Framingham. American Heart Journal 1986 112(2):432-437.
62) Sarwar N, Danesh J, Eiriksdottir G, Sigurdsson G, Wareham N, Bingham S, et al. Triglycerides and the Risk of Coronary Heart Disease. Circulation 2007 115(4):450-458.

63) Kannel WB, McGee DL. Diabetes and Cardiovascular Disease: The Framingham Study. JAMA 1979 241(19):2035-2038.
64) Freund KM, Belanger AJ, D'Agostino RB, Kannel WB. The health risks of smoking theframingham study: 34 years of follow-up. Annals of Epidemiology 1993 3(4):417-424.
65) Stary HC, Chandler AB, Glagov S, Guyton JR, Insull W, Rosenfeld ME, et al. A definition of initial, fatty streak, and intermediate lesions of atherosclerosis. A report from the Committee on Vascular Lesions of the Council on Arteriosclerosis, American Heart Association. Circulation 1994 89(5):2462-2478.
66) Hadi HAR, Carr CS, Al Suwaidi J. Endothelial Dysfunction: Cardiovascular Risk Factors, Therapy, and Outcome. Vascular Health and Risk Management 2005 1(3):183-198.
67) Su JB. Vascular Endothelial Dysfunction and Pharmacological Treatment. World Journal of Cardiology 2015 7(11):719-741.
68) Granger DN, Senchenkova E. Inflammation and the Microcirculation. San Rafael (CA): Morgan & Claypool Life Sciences; 2010. Chapter 7, Leukocyte–Endothelial Cell Adhesion. (pp.29-38)
69) Bobryshev YV, Ivanova EA, Chistiakov DA, Nikiforov NG, Orekhov AN. Macrophages and Their Role in Atherosclerosis: Pathophysiology and Transcriptome Analysis. Biomed Res Int. 2016 2016:9582430.
70) Gordon S, Martinez FO. Alternative activation of macrophages: mechanism and functions. Immunity. 2010 May 28 32(5):593-604.
71) Chistiakov DA, Bobryshev YV, Nikiforov NG, Elizova NV, Sobenin IA, Orekhov AN. Macrophage phenotypic plasticity in atherosclerosis: The associated features and the peculiarities of the expression of inflammatory genes. Int J Cardiol. 2015 Apr 1 184:436-445.
72) Yu XH, Fu YC, Zhang DW, Yin K, Tang CK. Foam cells in atherosclerosis. Clin Chim Acta. 2013 Sep 23;424:245-52.
73) Kunjathoor VV, Febbraio M, Podrez EA, Moore KJ, Andersson L, Koehn S, Rhee JS, Silverstein R, Hoff HF, Freeman MW. Scavenger receptors class A-I/II and CD36 are the principal receptors responsible for the uptake of modified low density lipoprotein leading to lipid loading in macrophages. J Biol Chem. 2002 277(51):49982-8.
74) Kunjathoor VV, Febbraio M, Podrez EA, Moore KJ, Andersson L, Koehn S, Rhee JS, Silverstein R, Hoff HF, Freeman MW. Scavenger receptors class A-I/II and CD36 are the principal receptors responsible for the uptake of modified low density lipoprotein leading to lipid loading in macrophages. J Biol Chem. 2002 277(51):49982-8.
75) Zhang L, Reue K, Fong LG, Young SG, Tontonoz P. Feedback Regulation of Cholesterol Uptake by the LXR–IDOL–LDLR Axis. Arterioscler Thromb Vasc Biol 2012 32(11):2541-2546.
76) Fan LM, Douglas G, Bendall JK, McNeill E, Crabtree MJ, Hale AB, et al. Endothelial Cell-Specific Reactive Oxygen Species Production Increases Susceptibility to Aortic Dissection. Circulation 2014 129(25):2661-2672.
77) Wang Y, Wang GZ, Rabinovitch PS, Tabas I. Macrophage Mitochondrial Oxidative Stress Promotes Atherosclerosis and Nuclear Factor-κB–Mediated Inflammation in Macrophages. Circ Res 2014 114(3):421-433.

78) Chistiakov DA, Bobryshev YV, Orekhov AN. Macrophage-mediated cholesterol handling in atherosclerosis. J Cell Mol Med 2016 20(1):17-28.
79) Xie J, Wang J, Tang T, Chen J, Gao X, Yuan J, et al. The Th17/treg functional imbalance during atherogenesis in ApoE−/− mice. Cytokine 2010 49(2):185-193.
80) Tay C, Kanellakis P, Hosseini H, Cao A, Toh B, Bobik A, et al. B cell and CD4 T cell interactions promote development of atherosclerosis. Frontiers in Immunology 2020; 10:3046.
81) Linton MF, Yancey PG, Davies SS, Jerome WG, Linton EF, Song WL, et al. The Role of Lipids and Lipoproteins in Atherosclerosis. In: Feingold KR, Anawalt B, Boyce A, Chrousos G, Dungan K, Grossman A, et al, editors. Endotext South Dartmouth (MA): MDText.com, Inc.; 2000.
82) Neville, B.W., Damm, D.D., Allen, C.M. and Chi, A.C. Oral & Maxillofacial Pathology. 4th Edition, WB Saunders, Elsevier, Missouri, 2013 604-605 (pp. 712, 723, 729)
83) Dietrich T, Sharma P, Walter C, Weston P, Beck J. The epidemiological evidence behind the association between periodontitis and incident atherosclerotic cardiovascular disease. J Periodontol. 2013 84(4 Suppl):S70-84.
84) Lockhart PB, Bolger AF, Papapanou PN, Osinbowale O, Trevisan M, Levison ME, Taubert KA, Newburger JW, Gornik HL, Gewitz MH, Wilson WR, Smith SC Jr, Baddour LM; American Heart Association Rheumatic Fever, Endocarditis, and Kawasaki Disease Committee of the Council on Cardiovascular Disease in the Young, Council on Epidemiology and Prevention, Council on Peripheral Vascular Disease, and Council on Clinical Cardiology. Periodontal disease and atherosclerotic vascular disease: does the evidence support an independent association?: a scientific statement from the American Heart Association. Circulation. 2012 125(20):2520-44.
85) Haffajee AD, Socransky SS. Attachment level changes in destructive periodontal diseases. J Clin Periodontol. 1986 13(5):461-75.
86) Humphrey LL, Fu R, Buckley DI, Freeman M, Helfand M. Periodontal disease and coronary heart disease incidence: a systematic review and meta-analysis. J Gen Intern Med. 2008 23(12):2079-86.
87) Rydén L, Buhlin K, Ekstrand E, de Faire U, Gustafsson A, Holmer J, Kjellström B, Lindahl B, Norhammar A, Nygren Å, Näsman P, Rathnayake N, Svenungsson E, Klinge B. Periodontitis Increases the Risk of a First Myocardial Infarction: A Report From the PAROKRANK Study. Circulation. 2016 133(6):576-83.
88) Chun YP, Chun KJ, Olguin D, Wang H. Biological foundation for periodontitis as a potential risk factor for atherosclerosis. J Periodont Res 2005 40(1):87-95.
89) Liu Z, Liu Y, Song Y, Zhang X, Wang S, Wang Z. Systemic Oxidative Stress Biomarkers in Chronic Periodontitis: A Meta-Analysis. Dis Markers 2014 2014:931083.
90) Loos BG, Craandijk J, Hoek FJ, Wertheim-van Dillen PM, van der Velden U. Elevation of systemic markers related to cardiovascular diseases in the peripheral blood ofperiodontitis patients. J Periodontol 2000 71(10):1528-1534.
91) Keaney Jr JF, Larson MG, Vasan RS, Wilson PWF, Lipinska I, Corey D, et al. Obesity and Systemic Oxidative Stress: Clinical Correlates of Oxidative Stress in the Framingham Study. Arterioscler Thromb Vasc Biol 2003 23(3):434-439.
92) Bermudez EA, Rifai N, Buring J, Manson JE, Ridker PM. Interrelationships Among Circulating Interleukin-6, C-Reactive Protein, and Traditional Cardiovascular Risk Factors in Women. Arterioscler Thromb Vasc Biol 2002 22(10):1668-1673.

93) Haraszthy VI, Zambon JJ, Trevisan M, Zeid M, Genco RJ. Identification of Periodontal Pathogens in Atheromatous Plaques. J Periodontol 2000 71(10):1554-1560.
94) López NJ, Quintero A, Casanova PA, Ibieta CI, Baelum V, López R. Effects of periodontal therapy on systemic markers of inflammation in patients with metabolic syndrome: a controlled clinical trial. J Periodontol. 2012 83(3):267-78.
95) Peng CH, Yang YS, Chan KC, Kornelius E, Chiou JY, Huang CN. Periodontal Treatment and the Risks of Cardiovascular Disease in Patients with Type 2 Diabetes: A Retrospective Cohort Study. Intern Med. 2017 56(9):1015-1021.
96) Offenbacher S, Beck JD, Moss K, Mendoza L, Paquette DW, Barrow DA, Couper DJ, Stewart DD, Falkner KL, Graham SP, Grossi S, Gunsolley JC, Madden T, Maupome G, Trevisan M, Van Dyke TE and Genco RJ. Results from the Periodontitis and Vascular Events (PAVE) Study: a pilot multicentered, randomized, controlled trial to study effects of periodontal therapy in a secondary prevention model of cardiovascular disease. Journal of periodontology. 2009 80:190-201.
97) Beck JD, Couper DJ, Falkner KL, Graham SP, Grossi SG, Gunsolley JC, Madden T, Maupome G, Offenbacher S, Stewart DD, Trevisan M, Van Dyke TE, Genco RJ. The Periodontitis and Vascular Events (PAVE) pilot study: adverse events. J Periodontol. 2008 79(1):90-6.
98) Nuvvula S, Chava VK, Nuvvula S. Primary culprit for tooth loss!! J Indian Soc Periodontol. 2016 20(2):222-4.
99) National Institute of Dental and Craniofacial Research. Prevalence of severe and non-severe (mild or moderate) periodontitis among dentate adults 30 years or older 2021. Available from: https://www.nidcr.nih.gov/research/data-statistics/periodontal-disease/adults
100) Hujoel PP, Drangsholt M, Spiekerman C, Derouen TA. Examining the link between coronary heart disease and the elimination of chronic dental infections. The Journal of the American Dental Association 2001 132(7):883-889.
101) Wu T, Trevisan M, Genco RJ, Dorn JP, Falkner KL, Sempos CT. Periodontal Disease and Risk of Cerebrovascular Disease: The First National Health and Nutrition Examination Survey and Its Follow-up Study. Arch Intern Med 2000 160(18):2749-2755.
102) Drzewoski J, Kasznicki J, Trojanowski Z. The role of "metabolic memory" in the natural history of diabetes mellitus. Pol Arch Med Wewn. 2009 Jul-Aug;119(7-8):493-500. PMID: 19776690.
103) Jax TW. Metabolic memory: a vascular perspective. Cardiovasc Diabetol. 2010 14;9:51.
104) Ceriello A, Ihnat MA, Thorpe JE: Clinical review 2: The "metabolic memory": is more than just tight glucose control necessary to prevent diabetic complications? J Clin Endocrinol Metab. 2009, 94:410-415.
105) Giacco F and Brownlee M. Oxidative stress and diabetic complications.

Circulation research. 2010 107:1058-70.

106) Miao F, Chen Z, Genuth S, Paterson A, Zhang L, Wu X, Li SM, Cleary P, Riggs

A, Harlan DM, Lorenzi G, Kolterman O, Sun W, Lachin JM, Natarajan R and Group

DER. Evaluating the role of epigenetic histone modifications in the metabolic memory of type 1 diabetes. Diabetes. 2014 63:1748-62

107) El-Osta A, Brasacchio D, Yao D, Pocai A, Jones PL, Roeder RG, Cooper ME and Brownlee M. Transient high glucose causes persistent epigenetic changes and altered gene expression during subsequent normoglycemia. The Journal of experimental medicine. 2008 205:2409-17.

108) Moore LD, Le T, Fan G. DNA methylation and its basic function. Neuropsychopharmacology. 2013 38(1):23-38.

109) Lyko F. The DNA methyltransferase family: a versatile toolkit for epigenetic regulation. Nat Rev Genet. 2018 19(2):81-92.

110) Rasmussen KD, Helin K. Role of TET enzymes in DNA methylation, development, and cancer. Genes Dev. 2016 30(7):733-50.

111) Okano, M., Bell, D. W., Haber, D. A. & Li, E. DNA methyltransferases Dnmt3a and Dnmt3b are essential for de novo methylation and mammalian development. Cell 1999 247–257.

112) Gruenbaum, Y., Cedar, H. & Razin, A. Substrate and sequence specificity of a eukaryotic DNA methylase. Nature 1982 295, 620–622.

113) Klimasauskas, S., Kumar, S., Roberts, R. J. & Cheng, X. HhaI methyltransferase flips its target base out of the DNA helix. Cell 1994 76, 357–369.

114) Ishida K, Kobayashi T, Ito S, Komatsu Y, Yokoyama T, Okada M, et al. Interleukin-6 Gene Promoter Methylation in Rheumatoid Arthritis and Chronic Periodontitis. J Periodontol 2012 83(7):917-925.

115) Zhang S, Crivello A, Offenbacher S, Moretti A, Paquette DW, Barros SP. Interferon-gamma promoter hypomethylation and increased expression in chronic periodontitis. J Clin Periodontol 2010 37(11):953-961.

116) Benakanakere M, Abdolhosseini M, Hosur K, Finoti LS, Kinane DF. TLR2 promoter hypermethylation creates innate immune dysbiosis. J Dent Res. 2015 94(1):183-91.

117) Q. Yang, Y. Zhao, Z. Zhang, J. Chen. Association of interleukin-6 methylation in leukocyte DNA with serum level and the risk of ischemic heart disease. Scand. J. Clin. Lab. Invest. 2016 76:291–295.

118) H. Zuo, Y. Guo, L. Che, X. Wu, Hypomethylation of Interleukin-6 Promoter is Associated with the Risk of Coronary Heart Disease., Arq. Bras. Cardiol. 2016 107:131–136.

119) Lund G, Andersson L, Lauria M, Lindholm M, Fraga MF, Villar-Garea A, Ballestar E, Esteller M, Zaina S. DNA methylation polymorphisms precede any histological sign of atherosclerosis in mice lacking apolipoprotein E. J Biol Chem. 2004 279(28):29147-54.

120) van Kampen E, Jaminon A, van Berkel TJ, Van Eck M. Diet-induced (epigenetic) changes in bone marrow augment atherosclerosis. J Leukoc Biol. 2014 96(5):833-41.

121) Christ A, Bekkering S, Latz E, Riksen NP. Long-term activation of the innate immune system in atherosclerosis. Semin Immunol. 201628(4):384-93.
122) Bekkering S, Joosten LA, van der Meer JW, Netea MG and Riksen NP. Trained innate immunity and atherosclerosis. *Curr Opin Lipidol*. 2013 24:487-92.
123) Kleinnijenhuis J, Quintin J, Preijers F, Joosten LA, Ifrim DC, Saeed S, Jacobs C, van Loenhout J, de Jong D, Stunnenberg HG, Xavier RJ, van der Meer JW, van Crevel R, Netea MG. Bacille Calmette-Guerin induces NOD2-dependent nonspecific protection from reinfection via epigenetic reprogramming of monocytes. Proc Natl Acad Sci U S A. 2012 109(43):17537-42.
124) Bekkering S, Quintin J, Joosten LA, van der Meer JW, Netea MG, Riksen NP. Oxidized low-density lipoprotein induces long-term proinflammatory cytokine production and foam cell formation via epigenetic reprogramming of monocytes. Arterioscler Thromb Vasc Biol. 2014 34(8):1731-8.
125) Saeed S, Quintin J, Kerstens HH, Rao NA, Aghajanirefah A, Matarese F, Cheng SC, Ratter J, Berentsen K, van der Ent MA, Sharifi N, Janssen-Megens EM, Ter Huurne M, Mandoli A, van Schaik T, Ng A, Burden F, Downes K, Frontini M, Kumar V, Giamarellos-Bourboulis EJ, Ouwehand WH, van der Meer JW, Joosten LA, Wijmenga C, Martens JH, Xavier RJ, Logie C, Netea MG and Stunnenberg HG. Epigenetic programming of monocyte-to-macrophage differentiation and trained innate immunity. Science. 2014 345:1251086.
126) Feingold KR. Introduction to Lipids and Lipoproteins. Endotext. South Dartmouth (MA): 2000– 2021 Jan 19.
127) Emini Veseli B, Perrotta P, De Meyer GRA, Roth L, Van der Donckt C, Martinet W, De Meyer GRY. Animal models of atherosclerosis. Eur J Pharmacol. 2017 Dec 5 816:3-13.
128) Ishibashi S, Brown MS, Goldstein JL, Gerard RD, Hammer RE, Herz J. Hypercholesterolemia in low density lipoprotein receptor knockout mice and its reversal by adenovirus-mediated gene delivery. J Clin Invest. 1993 Aug 92(2):883-93.
129) Yona S, Kim K, Wolf Y, Mildner A, Varol D, Breker M, et al. Fate Mapping Reveals Origins and Dynamics of Monocytes and Tissue Macrophages under Homeostasis. Immunity 2013 38(1):79-91.

130) Brown PM, Kennedy DJ, Morton RE, Febbraio M. CD36/SR-B2-TLR2 Dependent Pathways Enhance *Porphyromonas gingivalis* Mediated Atherosclerosis in the Ldlr KO Mouse Model. PLoS One 2015; 10(5): e0125126.

131) Huszar D, Varban ML, Rinninger F, Feeley R, Arai T, Fairchild-Huntress V, et al. Increased LDL Cholesterol and Atherosclerosis in LDL Receptor-Deficient Mice With Attenuated Expression of Scavenger Receptor B1. Arterioscler Thromb Vasc Biol 2000 20(4):1068-1073.

132) Basso F, Amar MJ, Wagner EM, Vaisman B, Paigen B, Santamarina-Fojo S, et al. Enhanced ABCG1 expression increases atherosclerosis in LDLr-KO mice on a western diet. Biochemical and Biophysical Research Communications 2006 351(2):398-404.

133) Lalla E, Lamster IB, Hofmann MA, Bucciarelli L, Jerud AP, Tucker S, Lu Y, Papapanou PN, Schmidt AM. Oral infection with a periodontal pathogen accelerates early atherosclerosis in apolipoprotein E-null mice. Arterioscler Thromb Vasc Biol. 2003 Aug 1 23(8):1405-11.

134) Febbraio M, Guy E and Silverstein RL. Stem cell transplantation reveals that absence of macrophage CD36 is protective against atherosclerosis. Arterioscler Thromb Vasc Biol. 2004 24:2333-8.

135) Marim FM, Silveira TN, Lima Jr DS, Zamboni DS. A Method for Generation of Bone Marrow-Derived Macrophages from Cryopreserved Mouse Bone Marrow Cells. PLoS One 2010 5(12):e15263.

136) Febbraio M, Podrez EA, Smith JD, Hajjar DP, Hazen SL, Hoff HF, Sharma K, Silverstein RL. Targeted disruption of the class B scavenger receptor CD36 protects against atherosclerotic lesion development in mice. J Clin Invest. 2000 105(8):1049-56.

137) Zhang X, Goncalves R and Mosser DM. The isolation and characterization of murine macrophages. Current protocols in immunology. 2008;Chapter 14:Unit 14 1.

138) RoadMap Epigenomics Project. RoadMap Epigenomics Project: Standards and Guidelines for Whole Genome Shotgun Bisulfite Sequencing . 2011; Available from: http://twww.roadmapepigenomics.org/files/protocols/data/dna-methylation/MethylC-SeqStandards_FINAL.pdf. [cited June 9,2020].

139) Kernaleguen M, Daviaud C, Shen Y, Bonnet E, Renault V, Deleuze JF, Mauger F, Tost J. Whole-Genome Bisulfite Sequencing for the Analysis of Genome-Wide DNA Methylation and Hydroxymethylation Patterns at Single-Nucleotide Resolution. Methods Mol Biol. 2018 1767:311-349.

140) Wang Z, Li X, Jiang Y, Shao Q, Liu Q, Chen B and Huang D. swDMR: A Sliding Window Approach to Identify Differentially Methylated Regions Based on Whole Genome Bisulfite Sequencing. PLoS One. 2015 10:e0132866

141) Sbodio JI, Snyder SH, Paul BD. Regulators of the transsulfuration pathway. Br J Pharmacol. 2019 176(4):583-593.

142) Vallance P. Homocysteine in Health and Disease. *J R Soc Med*. 2002 95(3):159.

143) Kim J, Lee G. Metabolic Control of m^6A RNA Modification. Metabolites. 2021 30 11(2):80.

144) Vizán P, Di Croce L, Aranda S. Functional and Pathological Roles of AHCY. Front Cell Dev Biol. 2021 9:654344.

145) James SJ, Melnyk S, Pogribna M, Pogribny IP, Caudill MA. Elevation in S-adenosylhomocysteine and DNA hypomethylation: potential epigenetic mechanism for homocysteine-related pathology. J Nutr. 2002 132(8 Suppl):2361S-2366S.

146) Xiao Y, Su X, Huang W, Zhang J, Peng C, Huang H, Wu X, Huang H, Xia M, Ling W. Role of S-adenosylhomocysteine in cardiovascular disease and its potential epigenetic mechanism. Int J Biochem Cell Biol. 2015 67:158-66.

147) Wu, X., Zhang, Y. TET-mediated active DNA demethylation: mechanism, function and beyond. Nat Rev Genet 2017 18, 517–534.

148) Hou LT, Liu CM, Liu BY, Lin SJ, Liao CS and Rossomando EF. Interleukin-1beta, clinical parameters and matched cellular-histopathologic changes of biopsied gingival tissue from periodontitis patients. Journal of periodontal research. 2003 38:247-54.

149) Miller CS, King CP, Jr., Langub MC, Kryscio RJ and Thomas MV. Salivary biomarkers of existing periodontal disease: a cross-sectional study. J Am Dent Assoc. 2006 137:322-9.

150) Linton MF, Atkinson JB, Fazio S. Prevention of atherosclerosis in apolipoprotein E-deficient mice by bone marrow transplantation. Science. 1995 17 267(5200):1034-7.
151) Ouweneel AB, Zhao Y, Calpe-Berdiel L, Lammers B, Hoekstra M, Van Berkel TJC, Van Eck M. Impact of bone marrow ATP-binding cassette transporter A1 deficiency on atherogenesis is independent of the presence of the low-density lipoprotein receptor. Atherosclerosis. 2021 319:79-85.
152) Klein SL, Flanagan KL. Sex differences in immune responses. Nat Rev Immunol. 2016 16(10):626-38.
153) Marriott I, Bost KL, Huet-Hudson YM. Sexual dimorphism in expression of receptors for bacterial lipopolysaccharides in murine macrophages: a possible mechanism for gender-based differences in endotoxic shock susceptibility. J Reprod Immunol. 2006 71(1):12-27.
154) Katsaros KM, Speidl WS, Demyanets S, Kastl SP, Krychtiuk KA, Wonnerth A, Zorn G, Tentzeris I, Farhan S, Maurer G, Wojta J, Huber K. G-CSF Predicts Cardiovascular Events in Patients with Stable Coronary Artery Disease. PLoS One. 2015 10(11):e0142532.
155) An G, Li B, Liu X, Zhang M, Gao F, Zhao Y, An F, Zhang Y, Zhang C. Overexpression of complement component C5a accelerates the development of atherosclerosis in ApoE-knockout mice. Oncotarget. 2016 7(35):56060-56070.
156) Wezel A, de Vries MR, Lagraauw HM, Foks AC, Kuiper J, Quax PH, Bot I. Complement factor C5a induces atherosclerotic plaque disruptions. J Cell Mol Med. 2014 18(10):2020-30.
157) Wang YK, Tang JN, Shen YL, Hu B, Zhang CY, Li MH, Chen RZ, Ge JB, Liu XB. Prognostic Utility of Soluble TREM-1 in Predicting Mortality and Cardiovascular Events in Patients With Acute Myocardial Infarction. J Am Heart Assoc. 2018 7(12):e008985.
158) Joffre J, Potteaux S, Zeboudj L, Loyer X, Boufenzer A, Laurans L, Esposito B, Vandestienne M, de Jager SC, Hénique C, Zlatanova I, Taleb S, Bruneval P, Tedgui A, Mallat Z, Gibot S, Ait-Oufella H. Genetic and Pharmacological Inhibition of TREM-1 Limits the Development of Experimental Atherosclerosis. J Am Coll Cardiol. 2016 Dec 27;68(25):2776-2793. doi: 10.1016/j.jacc.2016.10.015. PMID: 28007141.
159) Damås JK, Waehre T, Yndestad A, Otterdal K, Hognestad A, Solum NO, Gullestad L, Frøland SS, Aukrust P. Interleukin-7-mediated inflammation in unstable angina: possible role of chemokines and platelets. Circulation. 2003 107(21):2670-6..
160) Li R, Paul A, Ko KW, Sheldon M, Rich BE, Terashima T, Dieker C, Cormier S, Li L, Nour EA, Chan L, Oka K. Interleukin-7 induces recruitment of monocytes/macrophages to endothelium. Eur Heart J. 2012 33(24):3114-23.
161) Mihailovic PM, Lio WM, Yano J, Zhou J, Zhao X, Chyu KY, Shah PK, Cercek B, Dimayuga PC. IL-7R blockade reduces post-myocardial infarction-induced atherosclerotic plaque inflammation in $ApoE^{-/-}$ mice. Biochem Biophys Rep. 2019 May 19:100647.
162) Wang J, Zhao P, Gao Y, Zhang F, Yuan X, Jiao Y, Gong K. The Effects of Anti-IL-23p19 Therapy on Atherosclerosis Development in $ApoE^{-/-}$ Mice. J Interferon Cytokine Res. 2019 39(9):564-571.
163) Abbas A, Gregersen I, Holm S, Daissormont I, Bjerkeli V, Krohg-Sørensen K, Skagen KR, Dahl TB, Russell D, Almås T, Bundgaard D, Alteheld LH, Rashidi A, Dahl CP, Michelsen AE, Biessen EA, Aukrust P, Halvorsen B, Skjelland M. Interleukin 23 levels are increased in carotid atherosclerosis: possible role for the interleukin 23/interleukin 17 axis. Stroke. 2015 46(3):793-9.

164) Ziller MJ, Hansen KD, Meissner A and Aryee MJ. Coverage recommendations for methylation analysis by whole-genome bisulfite sequencing. Nat Methods. 2015 12:230-2, 1 p following 232.

165) Hiltunen MO, Turunen MP, Häkkinen TP, Rutanen J, Hedman M, Mäkinen K, Turunen AM, Aalto-Setälä K, Ylä-Herttuala S. DNA hypomethylation and methyltransferase expression in atherosclerotic lesions. Vasc Med. 2002 7(1):5-11.
166) Aavik E, Lumivuori H, Leppänen O, Wirth T, Häkkinen SK, Bräsen JH, Beschorner U, Zeller T, Braspenning M, van Criekinge W, Mäkinen K, Ylä-Herttuala S. Global DNA methylation analysis of human atherosclerotic plaques reveals extensive genomic hypomethylation and reactivation at imprinted locus 14q32 involving induction of a miRNA cluster. Eur Heart J. 2015 36(16):993-1000.
167) Guarrera S, Fiorito G, Onland-Moret NC, Russo A, Agnoli C, Allione A, Di Gaetano C, Mattiello A, Ricceri F, Chiodini P, Polidoro S, Frasca G, Verschuren MWM, Boer JMA, Iacoviello L, van der Schouw YT, Tumino R, Vineis P, Krogh V, Panico S, Sacerdote C, Matullo G. Gene-specific DNA methylation profiles and LINE-1 hypomethylation are associated with myocardial infarction risk. Clin Epigenetics. 2015 7:133.
168) Baba Y, Yagi T, Sawayama H, Hiyoshi Y, Ishimoto T, Iwatsuki M, Miyamoto Y, Yoshida N, Baba H. Long Interspersed Element-1 Methylation Level as a Prognostic Biomarker in Gastrointestinal Cancers. Digestion. 2018 97(1):26-30.
169) Yamada Y, Horibe H, Oguri M, Sakuma J, Takeuchi I, Yasukochi Y, Kato K, Sawabe M. Identification of novel hyper- or hypomethylated CpG sites and genes associated with atherosclerotic plaque using an epigenome-wide association study. Int J Mol Med. 2018 41(5):2724-2732..
170) Zaina S, Heyn H, Carmona FJ, Varol N, Sayols S, Condom E, Ramírez-Ruz J, Gomez A, Gonçalves I, Moran S, Esteller M. DNA methylation map of human atherosclerosis. Circ Cardiovasc Genet. 2014 7(5):692-700.
171) Foma AM, Aslani S, Karami J, Jamshidi A, Mahmoudi M. Epigenetic involvement in etiopathogenesis and implications in treatment of systemic lupus erythematous. Inflamm Res. 2017 66(12):1057-1073.
172) Jones PA. Functions of DNA methylation: islands, start sites, gene bodies and beyond. Nat Rev Genet. 2012 29 13(7):484-92.
173) Chen KC, Wang YS, Hu CY, Chang WC, Liao YC, Dai CY, Juo SH. OxLDL up-regulates microRNA-29b, leading to epigenetic modifications of MMP-2/MMP-9 genes: a novel mechanism for cardiovascular diseases. FASEB J. 2011 25(5):1718-28.
174) Tabaei S, Tabaee SS. DNA methylation abnormalities in atherosclerosis. Artif Cells Nanomed Biotechnol. 2019 Dec;47(1):2031-2041.
175) Jiang Y, Zhang H, Sun T, Wang J, Sun W, Gong H, Yang B, Shi Y, Wei J. The comprehensive effects of hyperlipidemia and hyperhomocysteinemia on pathogenesis of atherosclerosis and DNA hypomethylation in ApoE-/- mice. Acta Biochim Biophys Sin (Shanghai). 2012 44(10):866-75.
176) Zhang D, Chen Y, Xie X, Liu J, Wang Q, Kong W, Zhu Y. Homocysteine activates vascular smooth muscle cells by DNA demethylation of platelet-derived growth factor in endothelial cells. J Mol Cell Cardiol. 2012 53(4):487-96.

177) Rangel-Salazar R, Wickström-Lindholm M, Aguilar-Salinas CA, Alvarado-Caudillo Y, Døssing KB, Esteller M, Labourier E, Lund G, Nielsen FC, Rodríguez-Ríos D, Solís-Martínez MO, Wrobel K, Wrobel K, Zaina S. Human native lipoprotein-induced de novo DNA methylation is associated with repression of inflammatory genes in THP-1 macrophages. BMC Genomics. 2011 12:582.
178) Dong C, Chen J, Zheng J, Liang Y, Yu T, Liu Y, Gao F, Long J, Chen H, Zhu Q, He Z, Hu S, He C, Lin J, Tang Y, Zhu H. 5-Hydroxymethylcytosine signatures in circulating cell-free DNA as diagnostic and predictive biomarkers for coronary artery disease. Clin Epigenetics. 2020 12(1):17
179) Peng J, Yang Q, Li AF, Li RQ, Wang Z, Liu LS, Ren Z, Zheng XL, Tang XQ, Li GH, Tang ZH, Jiang ZS, Wei DH. Tet methylcytosine dioxygenase 2 inhibits atherosclerosis via upregulation of autophagy in ApoE-/- mice. Oncotarget. 2016 7(47):76423-76436.
180) Forman HJ, Zhang H, Rinna A. Glutathione: overview of its protective roles, measurement, and biosynthesis. Mol Aspects Med. 2009 30(1-2):1-12.
181) James SJ, Melnyk S, Pogribna M, Pogribny IP, Caudill MA. Elevation in S-adenosylhomocysteine and DNA hypomethylation: potential epigenetic mechanism for homocysteine-related pathology. J Nutr. 2002 132(8 Suppl):2361S-2366S.
182) Finkelstein JD. The metabolism of homocysteine: pathways and regulation. Eur J Pediatr. 1998 157 Suppl 2:S40-4.
183) Castro R, Rivera I, Martins C, Struys EA, Jansen EE, Clode N, Graça LM, Blom HJ, Jakobs C, de Almeida IT. Intracellular S-adenosylhomocysteine increased levels are associated with DNA hypomethylation in HUVEC. J Mol Med (Berl). 2005 83(10):831-6.
184) Xiao Y, Su X, Huang W, Zhang J, Peng C, Huang H, Wu X, Huang H, Xia M, Ling W. Role of S-adenosylhomocysteine in cardiovascular disease and its potential epigenetic mechanism. Int J Biochem Cell Biol. 2015 67:158-66.
185) Kerins DM, Koury MJ, Capdevila A, Rana S, Wagner C. Plasma S-adenosylhomocysteine is a more sensitive indicator of cardiovascular disease than plasma homocysteine. Am J Clin Nutr. 2001 74(6):723-9.
186) Xiao Y, Zhang Y, Wang M, Li X, Su D, Qiu J, Li D, Yang Y, Xia M, Ling W. Plasma S-adenosylhomocysteine is associated with the risk of cardiovascular events in patients undergoing coronary angiography: a cohort study. Am J Clin Nutr. 2013 98(5):1162-9.
187) Luo X, Xiao Y, Song F, Yang Y, Xia M, Ling W. Increased plasma S-adenosyl-homocysteine levels induce the proliferation and migration of VSMCs through an oxidative stress-ERK1/2 pathway in apoE(-/-) mice. Cardiovasc Res. 2012 Jul 15 95(2):241-50.
188) Xiao Y, Huang W, Zhang J, Peng C, Xia M, Ling W. Increased plasma S-adenosylhomocysteine-accelerated atherosclerosis is associated with epigenetic regulation of endoplasmic reticulum stress in apoE-/- mice. Arterioscler Thromb Vasc Biol. 2015 35(1):60-70.
189) Sipkens JA, Hahn NE, Blom HJ, Lougheed SM, Stehouwer CD, Rauwerda JA, Krijnen PA, van Hinsbergh VW, Niessen HW. S-Adenosylhomocysteine induces apoptosis and phosphatidylserine exposure in endothelial cells independent of homocysteine. Atherosclerosis. 2012 221(1):48-54.
190) Zhang H, Liu Z, Ma S, Zhang H, Kong F, He Y, Yang X, Wang Y, Xu H, Yang A, Tian J, Zhang M, Cao J, Jiang Y, Guo X. Ratio of S-adenosylmethionine to S-adenosylhomocysteine as a sensitive indicator of atherosclerosis. Mol Med Rep. 2016 14(1):289-300.

191) Loehrer FM, Tschöpl M, Angst CP, Litynski P, Jäger K, Fowler B, Haefeli WE. Disturbed ratio of erythrocyte and plasma S-adenosylmethionine/S-adenosylhomocysteine in peripheral arterial occlusive disease. Atherosclerosis. 2001 154(1):147-54.
192) Akalin FA, Baltacioğlu E, Alver A, Karabulut E. Lipid peroxidation levels and total oxidant status in serum, saliva and gingival crevicular fluid in patients with chronic periodontitis. J Clin Periodontol 2007 34(7):558-565.
193) Ambati M, Rani KR, Reddy PV, Suryaprasanna J, Dasari R, Gireddy H. Evaluation of oxidative stress in chronic periodontitis patients following systemic antioxidant supplementation: A clinical and biochemical study. J Nat Sci Biol Med 2017 8(1):99-103.
194) Liu Z, Liu Y, Song Y, Zhang X, Wang S, Wang Z. Systemic Oxidative Stress Biomarkers in Chronic Periodontitis: A Meta-Analysis. Dis Markers 2014:931083.
195) Kato T, Yamazaki K, Nakajima M, Date Y, Kikuchi J, Hase K, Ohno H, Yamazaki K. Oral Administration of Porphyromonas gingivalis Alters the Gut Microbiome and Serum Metabolome. mSphere. 2018 Oct 17 3(5):e00460-18.
196) Magnusson M, Lewis GD, Ericson U, Orho-Melander M, Hedblad B, Engström G, Ostling G, Clish C, Wang TJ, Gerszten RE, Melander O. A diabetes-predictive amino acid score and future cardiovascular disease. Eur Heart J. 2013 Jul 34(26):1982-9.
197) Ghasemi S. Cancer's epigenetic drugs: where are they in the cancer medicines? Pharmacogenomics J. 2020 20(3):367-379.